5-2019

Development of a lectin-Fc fusion protein with antiviral and anti-cancer activity.

Matthew William Dent
University of Louisville

DEVELOPMENT OF A LECTIN-FC FUSION PROTEIN WITH ANTIVIRAL AND ANTI-CANCER ACTIVITY

By
Matthew William Dent
B.S., Arizona State University, 2014
M.Sc., University of East Anglia, 2015

A Thesis Submitted to the Faculty of the University of Louisville School of Medicine in Partial Fulfillment of the Requirements for the Degree of

Master of Science in
Pharmacology and Toxicology

Department of Pharmacology and Toxicology
University of Louisville School of Medicine
Louisville, Kentucky

May 2019

DEVELOPMENT OF A LECTIN-FC FUSION PROTEIN WITH ANTIVIRAL AND ANTI-CANCER ACTIVITY

By

Matthew William Dent
B.S., Arizona State University, 2014
M.Sc., University of East Anglia, 2015

A Thesis Approved on

February 20, 2019

By the following Thesis Committee

_____
Dr. Nobuyuki Matoba

_____
Dr. Kenneth Palmer

_____
Dr. Sucheta Telang

_____
Dr. Jun Yan

_____
Dr. Donald Miller

DEDICATION

This thesis is dedicated to:

My mother and father, Dr. Jason C. Dent and Ms. Kimberly A. Dent, NP, for the years of support, inspiration, and opportunity that they have given me.

My wife, Dr. Milena Mazalovska, who has been by my side through it all and to whom I owe my sanity.

And lastly my mentor, Dr. Nobuyuki Matoba, and all my colleagues in the Biopharmaceutical Research Unit and the Department of Pharmacology and Toxicology for all their help and support.

ABSTRACT

DEVELOPMENT OF A LECTIN-FC FUSION PROTEIN WITH ANTIVIRAL AND ANTI-CANCER ACTIVITY

Matthew William Dent

February 20, 2019

This thesis describes the development of a novel lectin-Fc fusion protein and its antiviral and anti-cancer activity. The molecule, Avaren-Fc (AvFc), is a fusion of a variant of the actinomycete lectin actinohivin (Avaren) and the Fc region of human IgG1, and is selective for the terminal α1,2-mannose residues found at the ends of high-mannose-type glycans that can be found on the surface of certain heavily glycosylated viruses and cancer cells. Here, AvFc was found to be able to neutralize simian immunodeficiency virus as well as Hepatitis C virus with nanomolar IC_{50} values. Furthermore, AvFc recognizes a number of cell surface receptors and is capable of protecting mice against lung and flank B16F10 challenges primarily through Fc-mediated mechanisms. This work builds upon the framework developed by our group supporting the preclinical development of AvFc as a novel antiviral and anti-cancer protein.

TABLE OF CONTENTS

LIST OF FIGURES

LIST OF TABLES

CHAPTER I: INTRODUCTION

Glycosylation of Proteins

The modification of proteins through the addition of oligomeric carbohydrate chains (glycosylation) occurs in all domains of life and, in eukaryotes, is central to their processing in the endomembrane system. The importance of protein glycosylation is evident in the fact that nearly one fifth of all proteins are probably glycosylated [1]. This critical post- and co-translational modification is necessary for the proper folding and function of proteins that are destined for insertion into the plasma membrane or secretion into the extracellular space. The enzymes responsible for the addition and modification of the carbohydrate chains, termed *glycans*, are primarily found in the ER and Golgi apparatus. However, cross-species variation in the substrate, expression, and localization of these enzymes means that there is an incredible diversity in the glycoforms that can be generated. All of these, however, generally fall into one of two categories: asparagine (*N*) linked and serine/threonine (*O*) linked. While both are important to the function and structure of proteins, and although there are other categories of glycosylation (including lipid glycosylation), the focus of this section will be on *N*-linked glycosylation.

Description of *N*-glycans

The minimal sequence necessary for N-linked glycosylation is NXS/T (sequon), where X is any protein that is not proline. The presence of this sequence is not a guarantee that a glycan will be attached. In some cases, there are conformational or other constraints that preclude

glycosylation. As proteins are fed into the lumen of the ER, an enzyme called oligosaccharyltransferase (OST) covalently transfers the precursor glycan from the dolichol-linked precursor to the first asparagine in the sequon with a β glycosidic bond, which is modified enzymatically as the protein makes its way from the ER to the Golgi apparatus [2]. Proper *N*-glycosylation is important in signaling to the folding machinery that the protein is in the correct conformation and should be processed further, and disruptions in this process lead to protein degradation and ER dysregulation/unfolded protein response [3]. While there is a large amount of diversity in the resulting glycans, all of them share the same core structure consisting of two N-acetylglucosamine residues linked via an β1,4-glycosidic bond to mannose, which is linked to two other mannose residues via an α1,3- and an α1,6-bond. The resulting glycans can then be divided based on the identity of the residues attached to the core, of which there are three types: high-mannose, complex, and hybrid (**Figure 1**).

High-mannose glycans (HMGs) contain anywhere from 5 to 9 mannose residues (including the core structure) with no further additions to the chain. These are generally considered immature glycans, as they are rarely seen on fully processed glycoproteins. Complex glycans, conversely, have no mannose residues outside of the core and instead have two or more GlcNAc residues that extend from the two mannose arms forming “antennae”. Each of the two mannose arms in the core can accommodate the addition of more than two GlcNAc residues, resulting in tri- and tetra-antennary structures. In hybrid glycans only the α1,3-linked mannose branch of the core is extended by GlcNAc, while the α1,6-linked mannose branch remains in the high-mannose form. In addition, many mammalian glycans are modified with a core α1,6-fucose residue attached to the proximal GlcNAc residue, though this is not depicted. Unique to plants are core α1,3-fucose and β1,2-xylose residues, which connect at the proximal GlcNAc and the first mannose residue, respectively. Interestingly, while IgE antibodies against

these plant-specific structures have been detected in patients and are cross-reactive with plant foods, they have never been shown to induce clinical food allergy [4]. This is important, as they are the predominant glycan on proteins produced in plant-based expression systems, and much criticism of the system has been levied at the possible allergenicity of these molecules based on the unique glycans.

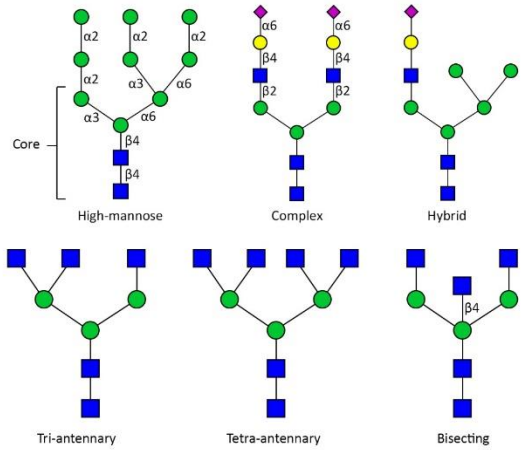

Figure 1 - Basic Structures of the Major Classes of N-Glycans. N-glycans are classified by their terminal residues and the number of branches in their structure, as shown above.

Aberrant Glycosylation in Cancer and Viruses

Changes to the normal pattern of *N*-glycosylation can be indicative of underlying disease, and aberrant glycoforms have been explored for their use as biomarkers and as therapeutic targets for cancer and certain viruses. Many glycoproteins belonging to enveloped viruses are heavily decorated with *N*-glycans. This glycosylation serves to both increase the affinity of the viral entry proteins to their cognate receptors on the host cell and to mask the underlying protein epitopes from the immune system [5]. A common modification is the over-representation of HMGs, which is seen in Influenza virus, HIV, Hepatitis C virus (HCV), West Nile Virus, MERS- and SARS coronavirus (CoV), Ebola virus, and HSV-2 among others [5]. One hypothesis is that this is due to changes in the cell metabolism associated with inflammatory signaling [6]. It is also possible that high expression of viral proteins produce steric hindrance

and prevent the trimming of certain occluded glycans [7]. Though the exact mechanism behind why HMGs are found in high quantities on these viruses is unknown, this phenomenon has led to the development of glycan-targeting viral entry inhibitors, in particular lectins, as possible antiviral therapeutics and prophylactic agents. Lectins are discussed in greater detail in the next section.

Alterations in the glycan profile of glycoproteins and glycosphingolipids are common features of cancer cells and are associated with increased cell viability and proliferation, tumor cell dissociation, migration, invasion, and modulation of the activity of signal transducers [8]. In the case of glycoproteins, the changes in glycosylation are mostly to *N*- or *O*-linked glycans. *O*-linked glycans are short carbohydrate chains attached to the hydroxyl oxygen of serine or threonine residues. Commonly identified changes to the *O*-glycan profile of cancer cells include the increased expression of rare Lewis antigens like sialyl Lewis and Lewsi^{Y} , Tn and sTn antigens, as well as truncated and branched O-glycans [9]. Changes to N-glycans include overexpression of core and terminal fucosylation, altered patterns of branching and bisecting GlcNAcs, and HMGs [9]. Despite the number of possible glycobiomarkers that have been identified, only a single glycan-targeting drug has been approved for use in humans (dinutuximab, which targets GD2 glycolipids expressed on neuroblastoma cells), necessitating the further development of therapies and diagnostics that can target them.

Lectins

Lectins are a broad class of proteins that recognize and reversibly bind to carbohydrates and glycoconjugates – sugar chains that can be found on the surface of other macromolecules including other proteins and lipids. In the late 19th century, lectins were very broadly referred to as hemagglutinins, or phytoagglutinins, since the erythrocyte agglutinating properties of these

proteins were first recognized in plant extracts. The first of these to be isolated from a plant extract is arguably the most famous (or infamous): ricin, an incredibly toxic lectin isolated from the castor bean (*Ricinus communis*) by Peter Hermann Stillmark in 1888 at the University of Dorpat in what is now Estonia [10]. At the time, lectins were only known as toxins and blood agglutinating agents. Studies with the earliest purified lectins, like ricin, abrin, and concanavalin A (Con-A) enabled researchers like Paul Ehrlich to determine that the immune system responds to individual antigens. Importantly, he determined that mice given sublethal doses of ricin eventually became immune to its effect (a discovery that would of course lead to the first vaccines). Since then, it has come to be understood that lectins are a very diverse and widespread group of proteins, and it is therefore quite difficult to generalize their structures and functions. In viruses and bacteria, they appear to play a role in host recognition and infection, while in plants they most notably act as defense mechanisms against pathogenic microorganisms. In animals and especially humans, lectins play important roles in cell signaling, adhesion, and trafficking as well as in immune regulation and pathogen recognition and response. This however is oversimplified. Of particular interest are lectins that can specifically recognize microbes, as these have tremendous implications for human health and have been studied with the intention of possibly developing new classes of therapeutics – the discovery of which has been accelerated by new genomics technologies. This section will briefly describe some of these lectins, their structure and function, and their development as biopharmaceuticals.

Antiviral Lectins

A number of lectins have been found to have antiviral activity by targeting glycans found on the surface of envelope glycoproteins, which have evolved as both a mechanism to increase

viral uptake by increasing affinity to host cell receptors as well as avoid the immune system by masking epitopes [11]. Coevolution of lectins with viruses has led to a large repertoire capable of recognizing non-self-glycans as a means of innate defense against the pathogens. These lectins generally consist of multiple repeated carbohydrate recognition domains (CRD), which increases their avidity for branched structures and allows them to more tightly bind to non-self-proteins. Many of the most well-described lectins in the literature target high-mannose glycan (HMG) structures, and consist of multiple CRDs that allow for tight binding to the glycoproteins of viruses such as HIV, Ebola virus, SARS-CoV, MERS-CoV, HCV, and many others [12-16]. All of these viruses contain heavily glycosylated host-cell-entry proteins that are primarily decorated with HMGs, which in normal human cells and glycoproteins are considered to be immature and not typically present in large quantities. When HMG-targeting lectins come into contact with these proteins and bind, disruption of the tertiary and quaternary structure of the viral glycoproteins leads to inhibition of entry and fusion, neutralizing the virus and allowing for immune clearance of the pathogens. These lectins are typically broadly active, making them attractive for therapeutic development as viral entry inhibitors despite the fact that many are toxic at higher doses.

A number of lectins with antiviral activity targeting HMGs have been isolated from bacteria, plants, and marine creatures. Of interest are actinohivin (AH, from actinomycetes), cyanovirin-N (CV-N, from a cyanobacterium), Griffithsin (GRFT, from red algae), BanLec (from bananas), microvirin (MVN), and scytovirin (from a cyanobacterium) [17-22]. Much work has been devoted to developing these as antiviral therapeutic or prophylactic agents and microbicides, especially for HIV, though data from *in vivo* protection models is limited, possibly due to the fact that many lectins are cytotoxic or mitogenic at doses that are clinically relevant. Of the lectins that have been isolated, GRFT has shown the most promise as an antiviral agent as it is broadly

acting and has limited toxicity when administered topically or systemically [23]. It has shown *in-vivo* activity against HIV, HSV-2, HCV, Japanese Encephalitis Virus, and SARS-CoV, and has been formulated into a rectal microbicide for a first-in-human clinical trial in 2019 (NIH Project Number: 5U19AI113182-03) [23-27]. CV-N has also shown promise as an anti-HIV agent in macaque SHIV challenge models [28, 29], and was well tolerated when administered rectally or vaginally. CV-N was formulated into a quick-dissolving vaginal suppository by Osel Inc, which made use of live recombinant *Lactobacillus jensenii* which constitutively expressed CV-N and was capable of protecting against SHIV transmission in macaques [30]. Interestingly, CV-N has also shown to have activity in a lethal mouse model of Ebola-Z infection [31]. Taken together, these data indicate that antiviral lectins may be a viable option for the prevention and treatment of certain viruses and that further *in vivo* studies should be performed.

Lectins as Cancer Therapy

Aberrant glycosylation has been detected in human cancers, resulting in the increased expression of rare antigens or changes in the proportions of others [32]. The utility of lectins as neoplastic therapeutic agents has been explored as the discovery of lectins that can bind these rare cancer glycoantigens has progressed. However, in general, there is more limited data on the *in vivo* effectiveness of lectins in cancer models. Plant lectins by far have been the most studied class of lectin with regards to anti-cancer activity, and several of them are derived from plants used in traditional Chinese medicine. Examples of such lectins are *Polygonatum odoratum* lectin (POL), Mistletoe lectin (ML), Con-A, and Soybean lectin. While each of these has shown some activity *in vitro*, the *in vivo* data is limited [33-40]. For instance, while protection against a xenogenic ovarian cancer in SCID mice was noted with ML, it showed no effect in an induced mouse bladder cancer model [41, 42]. Further *in vivo* study is warranted in order to determine

whether or not lectins are a viable option as a cancer therapeutic, and work must be done to demonstrate the selectivity of these lectins for cancer cells over normal human cells.

Transient Expression and Manufacturing of Biopharmaceuticals in Plants

Recombinant protein production, whether it be for pharmaceuticals or diagnostic reagents, has for the most part taken place in cell-culture-based systems (bacterial, insect, or mammalian cells). In these systems, transgenes are introduced to the target cells which mass-produce the protein of interest, which can then be harvested and purified to a final product. However, while considered the standard method of doing so, the time and cost associated with this method of production means that they can be difficult to employ in laboratory settings and that these drugs are only readily available in the developed world. This has led to the development of alternatives that may be more accessible to low-income areas and nations. To that end, plant-based expression (often referred to as "molecular pharming") offers several advantages over culture-based methods. Firstly, they are fast and robust, capable of producing comparable levels of protein in weeks rather than months [43, 44]. The speed at which new proteins can be made also greatly facilitates preclinical development, allowing for rapid testing of mutants and product variants. Secondly, they offer an improved safety profile, in that it is more unlikely to transfer human infectious material to the final product through soil and plant tissue than it is through mammalian cells or a culture medium containing components of animal origin. Lastly, they are more cost efficient and require significantly less capital investment for large scale production and scale-up [45]. To date, only a single recombinant pharmaceutical protein produced in plants has been approved by the FDA. The orphan drug, taliglucerase alfa (marketed by Protalix BioTherapeutics and Pfizer as ELELYSO®), is used as an enzyme replacement therapy for Gaucher's Disease and was approved in May 2012 [46]. With other

plant-made biopharmaceuticals entering clinical trials and at least one in Phase III (a quadrivalent influenza vaccine made by Medicago, see clinical trial record NCT03301051), plants are increasingly becoming recognized as a viable option for biopharmaceutical manufacturing.

The first reports of plant-derived pharmaceuticals were published in the late 80s and early 90s and demonstrated the production of immunoglobulins and vaccine antigens in transgenic tobacco plants [47, 48]. Much of the early research in molecular pharming then focused on the development of edible transgenic crop plants, especially nightshades like potato and tomato, for vaccine delivery [49, 50]. The idea at the time was that preparations of edible fruits or tubers containing vaccines could be made simply by growing the plant in the field from a transgenic seed, and the vaccine could then be given orally as opposed to with an injection. Requiring standard agricultural knowledge, rather than having expensive bioreactor facilities, meant that the technology to grow and distribute vaccines would be much more readily accessible to developing and other low-income countries. In addition, scale-up could easily be achieved by simply increasing the growth area. However, there are several caveats to using transgenic plants. The first and most problematic of these is that it can be difficult to generate a strong enough systemic immune response from orally delivered antigens without an adjuvant. The second is that expression levels can be variable from plant to plant even if they are genetically identical due to subtle changes in growth conditions, epigenetics, and gene silencing. This makes knowing the exact dose contained within the edible portion of the plant difficult and may preclude approval by the FDA, which has strict guidelines on vaccine dosing and preparation. The third is that transgenic plants can take a long time to make, as several generations are needed to transform, select, and then backcross to create the recombinant inbred lines that would then be grown on the field. Lastly, and most obviously, is that there is

significant public concern around genetically-modified crops which may make it difficult to market and sell such a product. Thus, much research has gone into developing alternatives.

Transient expression is a more rapid and robust way to produce recombinant protein in plants. Unlike with transgenics, transient gene expression constructs are not delivered to embryos but rather to fully grown, wild-type plants, the most common being a tobacco relative called *Nicotiana benthamiana*. This method offers many benefits in terms of yield, time, and reduced public concern (since food crops are not typically used). Two major types of vector have been developed to facilitate transient protein production, based on either full or deconstructed plant virus genomes [51]. With full virus-based vectors, the gene of interest (GOI) is inserted into a viral genome which then replicates and is translated as the virus spreads through the plant, producing the protein in large quantities as it goes. The most well-known example of a full viral vector is the GENEWARE® vector, based on tobacco mosaic virus (TMV) [52]. These vectors are useful because the virus containing the GOI can be stored in large quantities and can infect new plants with little effort, facilitating large scale production. However, infectious viral vectors typically cannot produce large-size proteins, as long GOI may prevent efficient viral RNA packaging and replication. Deconstructed viral vectors, on the other hand, do not place the GOI inside of a replication-competent viral genome. Instead, the major protein-coding genes are removed and the GOI is placed under the control of the viral promoter and terminator. Since there is no replicating virus with this type of vector, another method of delivery must be used to transform the host. This is done by the soil bacterium *Agrobacterium tumefaciens*, which is well known in agriculture as the causative agent of a disease called Crown Gall. The disease is characterized by large nodules in roots, branches and twigs, which form after the bacteria infects the plant cell and inserts a small piece of DNA (called transfer, or T-DNA, located on the tumor-inducing, or Ti, plasmid) into the host genome, which then produces a number of

virulence and growth factors for the bacterium [53]. Replacing the tumor-inducing genes on the T-DNA with deconstructed viral vector cassettes coding for pharmaceuticals allows for high-level production of protein in plants, a process called agroinfiltration. A well-known vector that is delivered via this method is magnICON® [54], which is a deconstructed vector based on TMV that does not produce replication competent virions. magnICON® has been especially successful at expressing therapeutic monoclonal antibodies and vaccines, highlighting the usefulness of this system [55-60]. A large number of other deconstructed vectors have been developed for the transient expression of recombinant proteins, as recently reviewed by Peyret et al. [51].

Therapy of HIV

HIV is a primarily-sexually-transmitted lentivirus that is the causative agent of acquired immunodeficiency syndrome, or AIDS, which is responsible for nearly a million deaths worldwide every year (WHO). HIV recognizes the CD4 receptor on immune cells, propagating inside them and ultimately leading to their death. As $CD4^+$ T cell counts diminish over several years to decades, the patient becomes more susceptible to infections and cancer, and will eventually succumb as the immune system becomes unable to function. Since the identification of the virus in the early 80's, advancements in antiretroviral therapy (ART) have improved to the point where most HIV^+ individuals on ART have nearly the same lifespan as people without and are less likely to transmit the virus to others. ART is a multi-drug regimen that is initiated at the time of diagnosis regardless of the symptoms. The US Department of Health and Human Services guidelines suggest that ART begin with 2 nucleoside-analog reverse transcriptase inhibitors (NRTIs) delivered with a protease inhibitor, a non-nucleoside reverse transcriptase inhibitor (NNRTI), or an integrase inhibitor (INSTI) (https://aidsinfo.nih.gov/contentfiles/lvguidelines/adultandadolescentgl.pdf). The ultimate

choice of drug depends on the patient's baseline resistance to therapy, which should be determined prior to the beginning of ART. The downside to ART is its high cost and the potential for resistance in the event a patient cannot or does not adhere to their regimen. Thus, there is a need to search for other treatment forms that can keep viral loads undetectable while improving adherence and lowering the number of adverse events.

The primary barrier to achieving a cure for HIV is the presence of latently infected resting $CD4^+$ memory T cells, which harbor the viral genes but do not actively produce virus [61, 62]. Upon cessation of ART, these reservoirs can become reactivated and the patient's viral load quickly rebounds. While various cure strategies have been implemented, including bone marrow transplant from HIV-resistant donors (as was the case with the Berlin Patient [63]), the focus of HIV cure research focuses around the use of latency reversal agents (LRAs) and agents that can target and kill reactivated latent cells. Among all of the drugs tested, the histone deacetylase inhibitors (HDACis) have shown the most clinical promise in their ability to reactivate latent reservoirs in humans, however none have been able to reduce the size of the latent reservoir alone [64]. In combination with HDACis, broadly neutralizing antibodies (bNAbs) against HIV have been used successfully in animal models to reduce the size of the latent reservoir and delay rebound (but not clear it entirely) [65]. This is a major step towards a cure, but more work needs to be done to identify LRAs that can more potently reactivate reservoirs and bNAbs that can more efficiently target infected cells and elicit antibody-dependent cell-mediated cytotoxicity (ADCC).

Therapy of Hepatitis C

HCV is an enveloped flavivirus that is spread through contaminated blood and causes liver damage, inflammation, and eventually cirrhosis and fibrosis. In most people, symptoms do

not occur until decades after the initial exposure, by which time liver is already severely damaged, and the patient may be in need of a transplant. Prior to 2011, the only treatment option for HCV patients was a combination regimen of pegylated interferon and ribavirin, a ribonucleoside guanosine analog, which could cure patients approximately 40-80% of the time but is also highly toxic with potentially severe side effects [66]. The advent of direct acting antivirals (DAAs) has made HCV an all but curable infection, with success rates reaching >90% with some genotypes [67]. DAAs inhibit specific parts of the HCV replication cycle primarily by targeting the viral protease (simeprevir, telaprevir) and the RNA-dependent RNA polymerase (sofosbuvir) [68]. As is the case with HIV, DAA regimens are typically multi-drug combination therapies whose composition depends on the genotype and inherent resistance of the strain in the patient. Despite the advances in treatment, it is likely that HCV-related liver cirrhosis will be the primary reason for liver transplant in the US for years to come. Furthermore, the cost of a DAA regimen can be upwards of $100,000 dollars, potentially limiting access to treatment. Particularly, in the case of liver transplant, the donor liver is reinfected with HCV almost immediately which can lead to accelerated cirrhosis and fibrosis of new organ. Typically, the patient cannot receive DAAs until they are off immunosuppressive drugs for a period due to potential interactions [69]. Therefore, there may be a need to develop an entry inhibitor that can protect donor livers from the virus.

Avaren-Fc

Previously, our lab has developed a novel fusion protein consisting of a lectin attached to the Fc region of human IgG1, called Avaren-Fc (AvFc). The lectin portion, called Avaren, is derived from the actinomycete lectin actinohivin, which was identified after screening for novel HIV inhibitors [70]. This lectin comprises three homologous tandem sugar-binding domains,

each of which being highly specific for the α1,2-linked mannose residues found in HMGs, allowing it to effectively neutralize HIV [71]. Unfortunately, when expressed recombinantly in plants actinohivin was prone to aggregation and yielded poorly. To increase the yield and the viability of actinohivin as a potential new drug, a number of mutations were made to neutralize the surface charge variation and decrease the propensity for aggregation (manuscript in preparation). Variant 8, which gave the highest yield while maintaining gp120-binding activity, was renamed *Avaren* (actinohivin variant expressed in *Nicotiana*, **Figure 2**). Furthermore, Avaren displayed similar overall structure as determined by circular dichroism and homology modeling (**Figure 3**). Avaren was then fused to the Fc portion of human IgG1 to further improve its activity by dimerization. The resulting protein, AvFc, retained the binding specificity of the original molecule while improving its affinity for gp120 (**Figure 4**) as well as its HIV neutralization activity (***Figure 5***). Additionally, the addition of the Fc region adds the possibility that AvFc can elicit antibody-dependent cell-mediated cytotoxicity (ADCC) and complement-dependent cytotoxicity (CDC) as well as have an antibody-like half-life by binding to the neonatal Fc receptor (FcRn). Induction of ADCC is particularly important in cancer therapy, making up an important part of a therapeutic mAb's mechanism of action (MOA) and improving its overall activity. As shown in **Figure 6**, AvFc can effectively bind to a number of different cancer cell-lines in a dose-dependent manner, with saturation occurring around 130 nM for most lines tested. Additionally, it can also elicit a stronger ADCC response against A549, MCF7, and RKO cells than can the approved therapeutic mAbs cetuximab and trastuzumab. This makes AvFc a novel first-in-class HMG-binding agent that combines both sugar recognition and Fc functions, justifying further study regarding its use as a possible anti-HIV or anti-cancer agent.

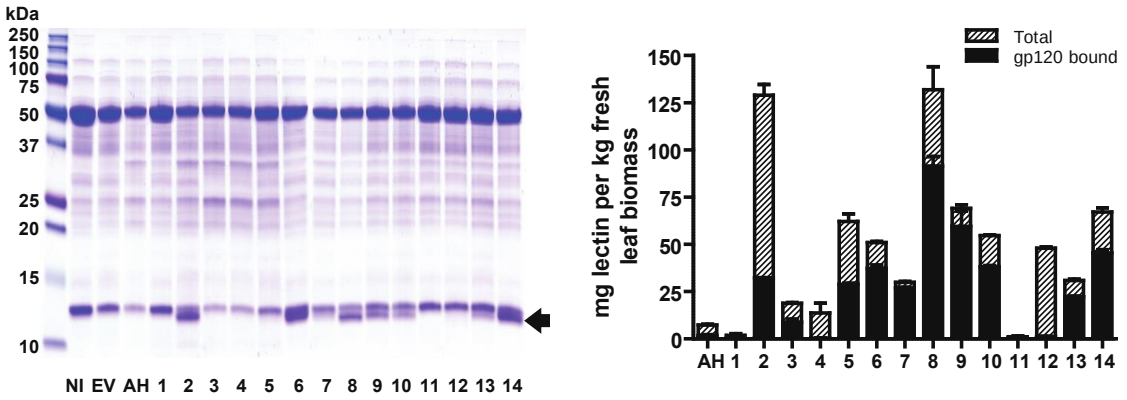


```
Actinohivin     1    ASVTIRNAQTGRLLDSNYNGNVYTLPANGGNYQRWTGP  38
                39   GDGTVRNAQTGRCLDSNYDGAVYTLPCNGGSYQKWLFY  76
                77   SNGYIQNVETGRVLDSNYNGNVYTLPANGGNYQKWYTG  114

Variant 8       1    ASGTIRNAETGRCLDSNYNGNVYTLPCNGGNYQRWTGP  38
                39   GDGTVRNAETGRCLDSNYDGAVYTLPCNGGSYQKWTGP  76
                77   GDGTIQNAETGRCLDSNYNGNVYTLPCNGGNYQKW-TG  114
```

Figure 2 - Yield and gp120 binding activity of actinohivin variants. Mutations were made in each of the three sugar-binding domains to decrease the overall hydrophobicity of the molecule and improve its production capability. Variant 8 gave the highest yield in a transient plant expression system while maintaining gp120-binding activity. This variant was renamed Avaren.

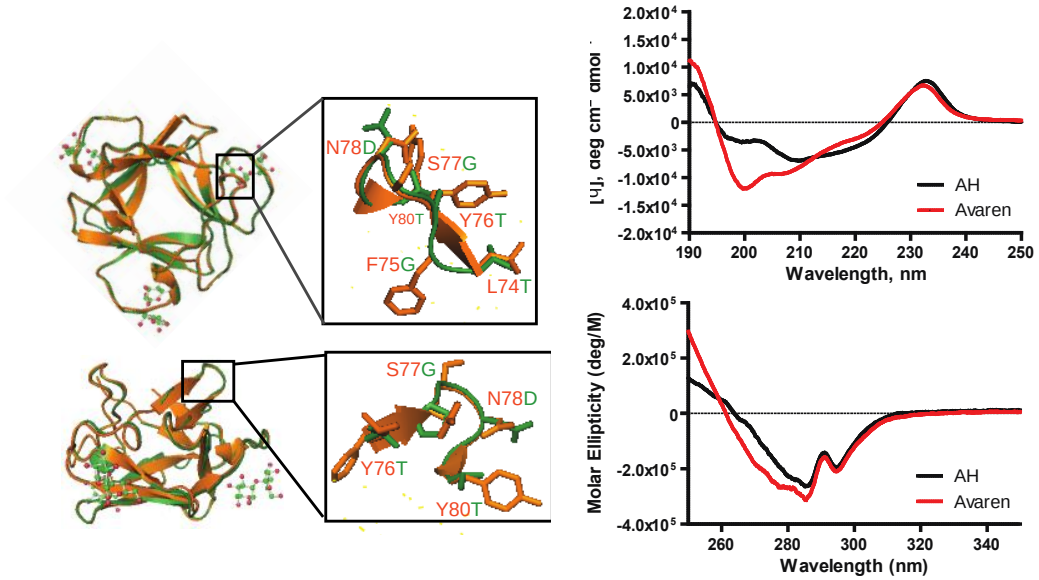

Figure 3 - Comparison of actinohivin and Avaren structure by homology modeling and circular dichroism. In the left panel, homology modeling shows that the predicted Avaren structure closely superimposes over the known crystal structure of actinohivin. In the right, circular dichroism analysis suggests that there is a mild increase in random coil structures. Nonetheless, the basic structure of the molecule appears to be the same.

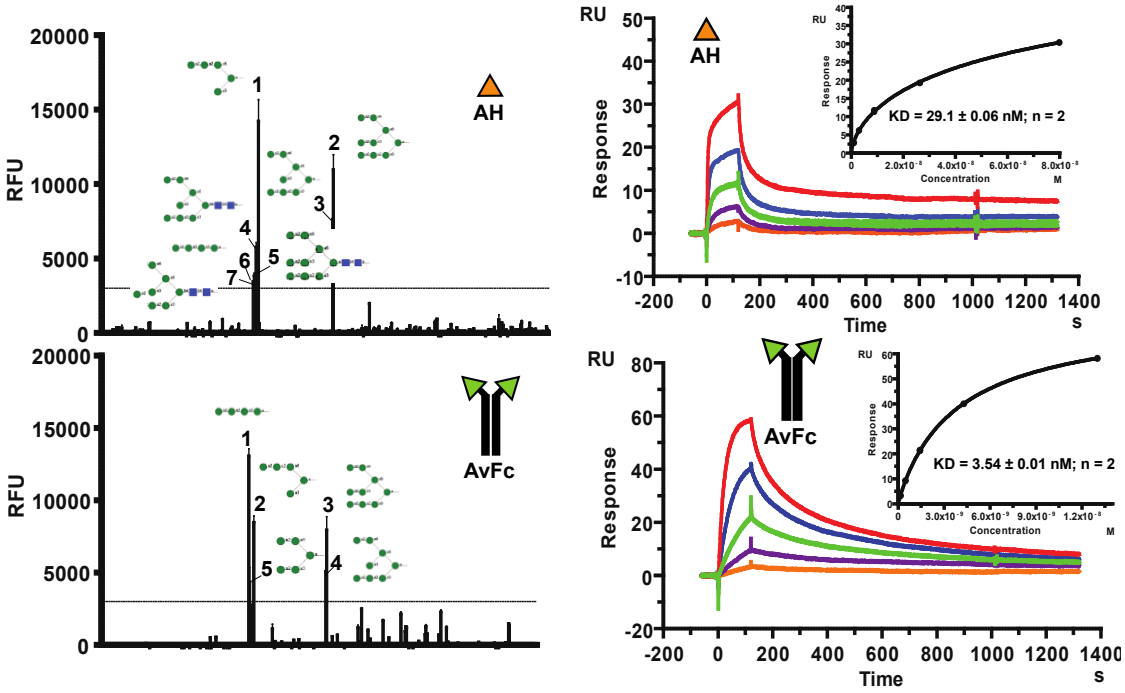

Figure 4 - Glycan array analysis and affinity to gp120 of AvFc and actinohivin. In the left panel, a glycan array analysis indicates that AvFc has similar specificity for HMGs, and that modification of the protein to Avaren did not alter the glycan-binding profile. In the right panel, modification to Avaren and dimerization through fusion to the Fc region of IgG1 improved the affinity of the molecule to HIV gp120 8-fold, from 29.1 nM to 3.54 nM.

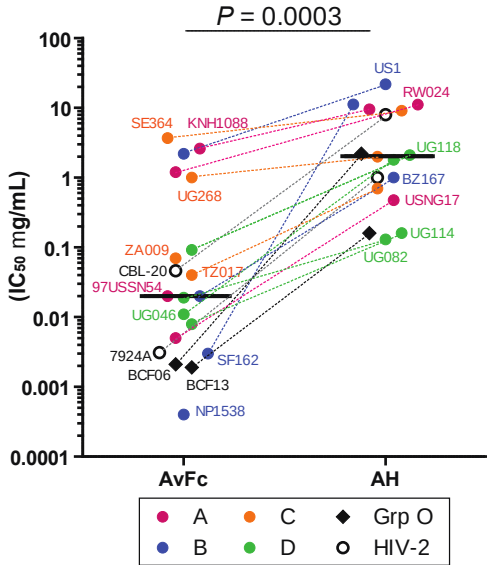

Figure 5 - HIV-neutralization activity of AvFc and actinohivin. The ability of AvFc and actinohivin to neutralize HIV was tested in a primary-cell-based neutralization assay. AvFc was capable of neutralizing multiple group M strains of HIV as well as group O and HIV-2, with an average IC_{50} value approximately 100-fold higher than that of actinohivin.

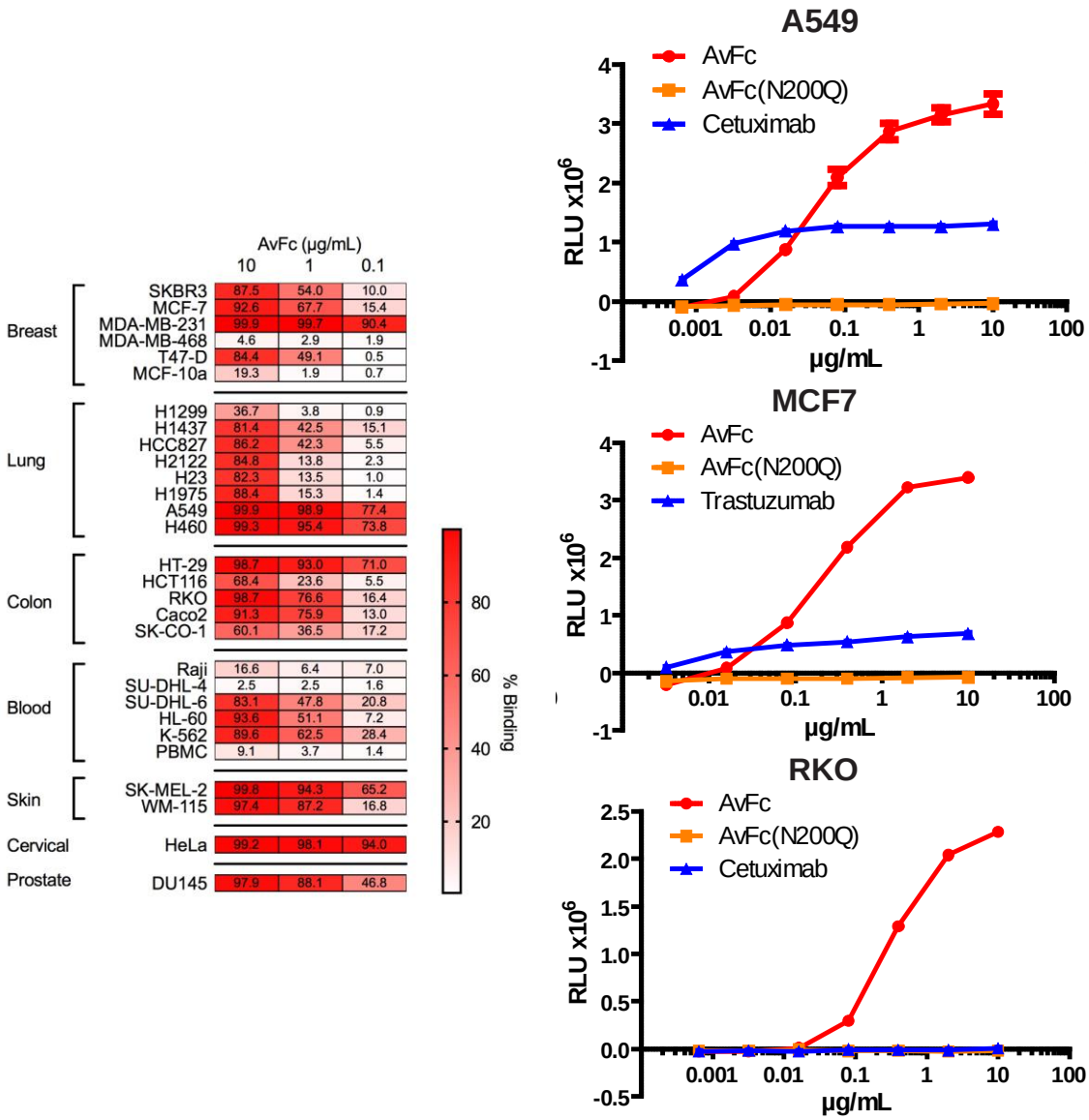

Figure 6 - Recognition of cancer cell-lines and induction of ADCC by AvFc. The left panel shows the binding of AvFc to a number of different cancer cell-lines originating from a variety of tissues. For most cell-lines shown, binding occurs in a dose dependent manner with saturation generally occurring around 10 µg/mL, or ≈ 130 nM. The right panel shows that AvFc effectively induces ADCC in a luciferase-expressing reporter-cell-based assay against three cancer cell-lines: A549, MCF7, and RKO. Furthermore, AvFc elicits a stronger response than the approved therapeutic mAbs cetuximab and trastuzumab.

CHAPTER II: EXPERIMENTAL PROCEDURES

Plant Growth

N. benthamiana was grown in a temperature-controlled room kept at a low humidity, with fluorescent lighting timed to a 16/8 hour day/night cycle. Seeding was done in new pots containing damp Jiffy Coco Mix, with 3-5 seeds per pot. Following seeding, plants were fertilized, covered with plastic wrap and incubated for 12 days, after which they were thinned and separated to a lower growth density. Fertilization and watering continued every other day until 4 weeks of age, at which point plants were ready for agroinfiltration.

Expression and Purification of AvFc and Variants

AvFc and variants were expressed in *N. benthamiana* using the MagnICON® vector system, which consists of three modules contained in separate plasmids: a 5' module, an integrase module, and a 3' module containing the gene of interest. Each plasmid was transformed into *A. tumefaciens* GV3101 by electroporation, and selection was performed using YenB agar (1% nutrient broth, 0.5% yeast extract) containing rifampicin (50 μg/mL) and ampicillin (100 μg/mL). A separate liquid culture made up of YenB, rifampicin, and ampicillin was then made for each of the three transformed cell lines and grown overnight at 30°C. When the cultures reached an OD_{600} of at least 1.0, they were spun down and resuspended in a small amount of MES buffer (10 mM MES, 10 mM $MgSO_4$ pH 5.5), and the OD_{600} remeasured. Each cell line was then mixed into a larger MES solution at a final OD_{600} of 0.03. This solution was then used for vacuum infiltration of the plants, which was done by submerging the plant upside down

into the solution inside a vacuum chamber and sealing it. A pump was used to create the vacuum, to which the plant and solution was exposed to for 3 minutes. Afterwards, the pressure was relieved slowly, at which point the bacteria solution infiltrated the leaf tissue. This procedure was repeated for each plant. After infiltration, plants were returned to the growth chamber and incubated for 7 days.

At 7 days post infiltration (dpi), leaf tissue was harvested from the plants and homogenized using a Waring blender with extraction buffer (20 mM NaPi, 40 mM Ascorbic acid, pH 7). This crude extract was filtered through a layer of cheesecloth and miracloth, and the filtrate was centrifuged at 15,000 xg for 15 minutes at 4°C. Concentrated HCl was used to lower the pH of the supernatant to 5.2, which was spun again at 15,000 xg for 10 minutes at 4°C. Then, the pH of the supernatant was rapidly brought back to pH 7 and spun again at 15,000 xg for 10 minutes at 4°C. This clarified extract was then filtered with a 0.2 µm vacuum filter for purification by Fast Protein Liquid Chromatography (FPLC).

FPLC was performed using the AKTA Pure system (GE Healthcare Life Sciences) and a two-step purification procedure. The first step was affinity chromatography using a prepacked 5 mL Protein A column (HiTrap® MabSelect™ SuRe™, GE Healthcare Life Sciences #GE11-0034-94). For murine AvFc IgG1, a Protein G column (HiTrap Protein G HP, GE Healthcare Life Sciences #17040501) was used instead of Protein A, as murine IgG1 does not bind to it. However, the protocol for both is the same. First, the column was equilibrated with 5 column volumes (CV) of extraction buffer. Clarified plant extract was then loaded onto the column at 2.5 mL/min, giving a residence time of 2 minutes. After sample loading, the column was washed with 10 CV of Protein A wash buffer (5 mM NaPi, pH 7) and then eluted with 10 CV of Protein A elution buffer (2 M arginine, pH 3) into 5 mL fractions. Fractions containing the protein (typically 2-5) were neutralized with 1 M tris and then pooled together for further purification.

The second round of purification was performed with a 5 mL prepacked ceramic hydroxyapatite column (Bio-Scale Mini CHT Type II 40 µm, Bio-Rad #7324334). Pooled fractions from the previous step were diluted with water until the conductivity of the solution dropped below ≤ 10 mS/cm. Then, the CHT column was neutralized with 1 CV of a neutralization buffer (250 mM NaPi pH 7) and equilibrated with 10 CV of CHT wash buffer (5 mM NaPi pH 7). Sample was loaded at a rate of 2.5 mL/min giving a 2 min residence time, after which the column was washed with 5 CV of CHT wash buffer. Protein was eluted from the column using a linear step from 0% to 100% CHT elution buffer (5 mM NaPi pH 7, 800 mM NaCl) over 10 CV. The elutions were collected as 10 mL fractions. Finally, the column was stripped with CHT stripping buffer (5 mM NaPi pH 7, 4 M NaCl). Fractions were analyzed by SDS-PAGE, and protein-containing fractions were pooled and concentrated on a 10 kDa MWCO Amicon® filter (Millipore #C7715). The same filters were also used to exchange the buffer for the final AvFc formulation buffer (30 mM histidine, 100 mM sucrose, 100 mM NaCl, pH 7.4). Endotoxin was removed from the final purified product using phase separation with Triton X-114. Briefly, 1% Triton X-114 was added to the protein, which was then heated to 37°C and spun in a centrifuge. The uppermost aqueous layer was taken, and endotoxin removal was confirmed using the Limulus Amebocyte Lysate test (Charles River Endosafe®-PTS). Final product had an endotoxin level of <1 units/mg of AvFc and was stored in aliquots at -80°C.

HIV gp120 ELISA

Clear 96-well plates were coated with 0.3 µg/mL of HIV gp120 CM235 (NIH Aids Reagent Program #2968) in carbonate buffer pH 9.6 and incubated overnight at 4°C. Plates were then blocked with PBST containing 5% dry milk for 30 minutes at 37°C. AvFc or other variants were then added to the plate at 13 nM (1 µg/mL) and serially diluted down the plate 1:5, then

incubated for 1 hour at 37°C. AvFc was then detected with a goat anti-human IgG HRP (Santa Cruz Biotechnology #2907) at a dilution of 1:10,000 for 1 hour at 37°C. Between each step, plates were washed with PBST 3 times. After a final washing, plates were incubated for no more than 4 minutes with TMB substrate (Seracare #5120-0075). At that time, the reaction was stopped with a solution of 0.6 N sulfuric acid and 1 N HCl and read on a BioTek plate reader at 450 nm. Absorbance at 450 nm was plotted against the log of the concentration and fit with a 4-parameter non-linear regression with GraphPad Prism to calculate EC_{50}. The lower limit of detection (LLOD) and lower limit of quantification (LLOQ) were calculated as the background signal plus 3 times the standard deviation of the background or 10 times the standard deviation, respectively, and interpolated using the non-linear regression.

Culture of Primary Simian Immunodeficiency Virus (SIV) Strains

SIV [what strains?] was propagated in CEMx174 suspension cells (NIH Aids Reagent Program #272), which is a fusion cell line formed from the human T cell line CEM and the human B cell line 721.174 that is commonly used for propagation of SIV, SHIV, and HIV [need citations]. These cells are cultured in RPMI 1640 supplemented with 10% FBS to a density of approximately 1-2 x 10^6 cells/mL. For infection, approximately 5 x 10^6 cells were pelleted, resuspended in 1 mL of the virus (pulled from frozen storage), then incubated at 37°C for 1 hour. Some cells were also set aside to remain uninfected for future use. Afterwards, cells were diluted in growth medium and incubated at 37°C with 5% CO_2. Each day, cell cultures were monitored for growth and virus-induced cytotoxicity and beginning on day 3, cultures were assayed for the presence of the SIV capsid protein p27 using a commercial ELISA kit (XpressBio #SK845). Uninfected cells were fed to the virus cultures if a slowdown in growth or virus production was noted, and upon confluency cells were split into new flasks by dilution with fresh medium to keep propagating virus. When

the concentration of p27 was ≥ 100 ng/mL, cell-free virus stocks were made by spinning down cells at 1000 xg for 5 minutes, collecting the supernatant, and storing in 1 mL internally-threaded cryovials at -80°C.

SIV Titration for Neutralization Assays

To determine the amount of virus needed for the SIV neutralization assay, a titration assay with TZM-bl cells as the host was used. TZM-bl is a recombinant Hela cell line that expresses CD4 and CCR5 and contains a Tat-activated luciferase gene, making it useful to monitor HIV or SIV infection [72]. To a white 96 well plate, 50 µL of TZM-bl growth medium (Dulbecco's Modified Eagle Medium, DMEM, supplemented with 10% FBS) was added to each well in columns 2-12, leaving column 1 empty. Then, 62.5 µL of neat virus was added to at least 4 wells in column 1. This allows for the testing of two viruses per plate. Virus was serially diluted 1:5 across the plate from column 1 to 11 by transferring 12.5 µL between wells and discarding 12.5 µL from the last column. Then, 150 µL of TZM-bl cells at a concentration of 6.7×10^4 cells/mL in growth medium were added to each well on the plate (10,000 cells/well) and incubated for 2 days at 37°C with 5% CO_2. After this incubation period, plates were removed from the incubator and 100 µL of medium was removed from each well. To each well, 100 µL of luciferase reagent (BriteLite Plus Reporter Gene Assay System, Perkin Elmer #6066761) was then added and incubated for 1 minute, after which plates were read on a BioTek plate reader. The viral titer ($TCID_{50}$) was calculated using the Reed and Muench method [73]. A relative luminescence (RLU) value greater than 2.5x the cell-only control value was considered positive for infection. In addition, a dilution of virus that would give an RLU value of at least 10x greater than the cell only control was chosen for use in the neutralization assay.

SIV Neutralization Assay

The SIV neutralization assay was carried out on a white opaque 96-well plate with TZM-bl cells as the host cell. This format allows for the testing of three samples with 8 dilutions and includes no-drug, no-drug/virus, and no-drug/virus/cell control columns. To begin, 50 µL of TZM-bl growth medium was added to Rows B-H in columns 1-9. 50 µL of medium was also added to column 10 (for the no-drug control), 100 µL to column 11 (for the no-virus control), and 200 µL to column 12 (blank). AvFc was prepared in growth medium at 4x the desired starting concentration and 62.5 µL of drug was added to at least 3 wells in row A for triplicate analysis. As a negative control, the control lectibody $AvFc^{lec-}$, which contains mutations in the Avaren portion of the protein that eliminates sugar-binding (Y32A, Y70A, Y108A), was prepared and plated in a similar manner. Each drug was serially diluted 1:5 down the plate from Row A to H by transferring 12.5 µL between wells and discarding 12.5 µL from the last dilution. SIV, either smE660, mac239, or mac251 strain was diluted in growth medium to a dilution 4x higher than the desired dilution. 50 µL of virus was then added to each well in columns 1-10. The plate was incubated for 1 hour at 37°C and 5% CO_2. After this incubation step, TZM-bl cells are harvested and resuspended to a concentration of 1 x 10^5 cells/mL in growth medium. 100 µL of these cells are then added to every well in columns 1-11 (10,000 cells/well) and the plates are incubated for 2 days at 37°C with 5% CO_2. After two days, 100 µL of medium is removed from each well and 100 µL of luciferase reagent is added to each well, then the plate is read on a BioTek plate reader. Inhibition was counted as a decrease in RLU. The average RLU value of the no-drug/virus controls were subtracted from each well as background. Sample RLU values were then converted to percent inhibition using the following formula:

$$Percent\ inhibition = 1 - \frac{RLU_{sample}}{RLU_{nodrug}} * 100$$

Percent inhibition vs. sample concentration was then plotted with GraphPad Prism. The 50% inhibitory concentrations (IC_{50}s) for each sample were calculated using a 4-parameter non-linear regression analysis.

Flow Cytometry of SIV-Infected Mesenteric Lymph Node Cells

Cells isolated from rhesus macaque mesenteric lymph nodes (MLNs) were infected with SIVmac251 and cultured in RPMI 1640 supplemented with 10% FBS and 40 U/mL of human IL-2 (Tonbo Biosciences #21-8029). Uninfected cells were also cultured as a control. Cultures were monitored for p27 expression using a commercial ELISA kit as described above. After infection was confirmed by a positive ELISA test, cells were harvested and blocked with a solution of PBST, 3% BSA, and human Fc block (BD #564219) for 30 minutes on ice. Cells were then washed and stained with 1 or 10 µg/mL AvFc and then with a goat anti-human IgG-FITC secondary (Abcam #ab97224). Flow cytometry was performed on a BD FACScan. Cell populations were gated for live lymphocytes and unstained cells were used to determine the background fluorescence.

Pharmacokinetic Analysis of AvFc in Rhesus Macaques

Two adult female rhesus macaques (RYL15 and RBL15), weighing 5.76 and 5.72 kg, were given a 21 mg bolus intravenous injection of AvFc equaling a dose of 3.6 and 3.7 mg/kg. Blood was sampled at 0, 0.5, 1, 2, 4, 8, 24, 48, and 72 hours and placed in serum tubes containing EDTA. Serum was then separated from whole blood through centrifugation and assayed for AvFc with a gp120 ELISA. To determine whether or not there was any matrix interference, a standard gp120 ELISA was performed as described above by spiking varying concentrations of normal macaque serum (Innovative Research #IRS-SER) with AvFc and assessing any change in EC_{50},

LLOD, or LLOQ using GraphPad Prism. Once any interference was established, gp120 ELISA with purified AvFc as a standard was used to extrapolate the concentration of drug in the PK samples. The concentration of AvFc in the serum was plotted against time and PK parameters estimated using PK Solver [74].

Production of HCV

Cell culture HCV (HCVcc) can be produced by transfecting Huh7.5 cells with RNA coding for the viral genes. The DNA construct containing the sequence for the J6/JFH fusion virus (genotype 2a) and the Huh7.5 cell line was obtained from Apath, LLC. All washing and centrifugation steps take place at 4°C, and materials are kept on ice unless otherwise specified. Huh7.5 cells were first grown in a large flask to 90% confluency in DMEM supplemented with 10% FBS, after which they were washed with PBS, trypsinized, and resuspended in 10-15 mL of ice-cold RNase-free PBS. At this point, the cells were counted and washed two more times with RNase-free PBS. For the last wash, cells were resuspended in RNase-free PBS to a final concentration of 1.5×10^7 cells/mL. At the same time, viral RNA was generated from the DNA construct using the mMessage mMachine T7 RNA transcription kit (ThermoFisher #AM1344). 1 to 10 µg of the RNA was then placed in an RNA-free 1.5 mL tube and mixed with 0.4 mL of the cell suspension. This mixture was transferred to a 4 mm cuvette and electroporated at 270 V and a capacitance of 950 µF and then left at room temperature for 10 minutes. Afterwards, the transformed cells were transferred to a 75 cm^2 flask containing 11.6 mL of growth medium and incubated at 37°C and 5% CO_2 until they became > 85% confluent. At this point the medium was collected, and the viral titer determined. This virus can also be used to propagate more in the future.

TCID50 Assay for HCVcc

The viral titer was determined using an immunofluorescence assay. Black 96-well plates were seeded with 5000 cells/well and incubated overnight to allow their attachment. The next day, serial dilutions (1:10) of virus beginning from neat virus were added to the wells, and the plates were incubated for 72 hours at 37°C with 5% CO_2. After this incubation period, the medium was aspirated and disposed of, and the cells were fixed and permeabilized using an ice-cold 1:1 solution of methanol and acetone. The solution and cells were allowed to equilibrate to room temperature for 10 to 20 minutes, after which they were washed twice with PBS. Immunostaining was done with an anti-HCV core antigen FITC conjugate monoclonal antibody (Abcam ab123076) at a 1:1000 dilution in 3% BSA/PBS for 2 hours at room temperature. The cells were then washed and stained with DAPI (Abcam ab228549) for 10 minutes at 4°C. Lastly, the infected cells were visualized using a fluorescence microscope. The number of foci in each well was counted to determine the endpoint titer and the $TCID_{50}$ was calculated using the Reed and Muench method [73].

HCVcc Neutralization Assay

The HCV neutralization assay was carried out using an immunofluorescence assay on a 96-well plate. First, the plate was seeded with 5000 cells/well and incubated overnight. The next day, cells were washed and AvFc was added in 100 µL of growth medium to the plate in 1:5 serial dilutions beginning at 2x the desired starting concentration (130 nM). One column of wells was left with no drug to serve as a positive control. After, HCVcc was added to each well at a multiplicity of infection (MOI) of 0.1, and the plates were incubated for 72 hours at 37°C with 5% CO_2. At that time, the cells were fixed and stained as described above, and the number of infected cell foci (foci forming units, FFU) per well were counted. Inhibition was counted as a

reduction in FFU. The counts were then converted to percent inhibition using the following formula:

$$Percent\ inhibition = 1 - \frac{FFU_{sample}}{FFU_{nodrug}} * 100$$

Percent inhibition vs. sample concentration was then plotted with GraphPad Prism. The 50% inhibitory concentrations (IC_{50}s) for each sample were calculated using a 4-parameter non-linear regression analysis.

Flow Cytometry Analysis of AvFc Binding to B16F10 Cells

B16F10 cells were grown in DMEM supplemented with 10% FBS. For flow cytometric analysis, cells were harvested with a 0.25% trypsin/EDTA solution and washed with PBS. Cells were then stained with a PBS control, AvFc at 1.3, 13, or 130 nM or $AvFc^{lec-}$ at 130 nM, and a goat anti-human Fc-FITC at 1:250. All incubations were carried out on ice for half an hour in the dark. Cells were the analyzed using a BD FACScan and the FlowJo software. Live cells and cells positive for FITC were gated based on the PBS control, and the results were analyzed in GraphPad Prism.

ADCC Reporter Assay

The ADCC assay was carried out using the Promega ADCC Bioassay Effector Cells, Propagation Model (Promega #G7102). For the assay, the B16F10 target cells were grown as described above. At the same time the effector cell line, Jurkat-FcγRIIIa-luc, was grown in RPMI 1640 supplemented with 10% FBS, 100 µg/mL hygromycin, 250 µg/mL antibiotic G-418 sulfur solution, 1 mM sodium pyruvate, and 0.1 mM MEM non-essential amino acids. On a 96-well plate, 10,000 B16F10 cells were plated per well and allowed to adhere overnight. The next day,

dilutions of AvFc were prepared on a separate plate and added on top of the cells in addition to 150,000 effector cells. The plates were incubated overnight at 37°C, after which the cells were lysed. Lysate was mixed with luciferase assay reagent (Promega #E1500) and luminescence read on a plate reader. RLU values from the plate reader were converted to fold induction based on the background signal, plotted against the concentration, and fit with a non-linear regression using GraphPad Prism.

B16F10 Melanoma Lung Metastasis Model

For the mouse model of melanoma lung metastasis only 8-10-week-old C57bl/6 mice were used, and B16F10 cells were grown as described above. On day 0, animals received their first intraperitoneal dose of either vehicle (n=40), 25 mg/kg AvFc (n=30), or 25 mg/kg AvFc^{lec-} (n=10). 2-4 hours later, 2.5 x 10^5 B16F10 cells were injected intravenously into each animal. Dosing continued every other day for a total of 6 doses. On day 21 animals were euthanized and their lungs were removed for analysis. For each lung, the number of black tumor nodules was noted. The same model was also used with a delayed treatment of AvFc or vehicle (n=10 each), which began on day 7 and continued every other day for a total 6 doses. Animals were monitored until their death or until their condition necessitated euthanasia.

B16F10 Flank Tumor Model

In this model, 20 8-10-week-old C57bl/6 mice were shaved and given 2.5 x 10^5 B16F10 cells in the hind left flank. Treatment with AvFc intraperitoneally at 25 mg/kg or vehicle began when the tumors became visible (approximately 50 mm^3), at 5 days post injection. The size of the tumor was measured each day with digital calipers, and animals were euthanized when the

tumor size reached 1500 mm^3. Dosing continued every other day until study termination at day 14.

Proteomic Analysis of AvFc Binding Partners on Cancer Cells

Co-immunoprecipitation was used to isolate potential binding partners of AvFc on the surface of cancer cells. Four different cancer cell lines were chosen for analysis, representing two lung cancers (H460 and A549) and two blood cancers (HL-60 and K562). The two lung cancer cell lines were grown using DMEM supplemented with 10% FBS, while the blood cancer cell lines were grown in suspension with RPMI 1640, supplemented with 10% FBS. Co-immunoprecipitation was performed using the Pierce™ Co-Immunoprecipitation Kit (ThermoFisher #26149) according to the kit instructions. Briefly, AvFc or $AvFc^{lec-}$ was covalently linked to an agarose resin. Then, 1 x 10^7 cells were lysed using a buffer containing 1% NP-40 and 1X Halt™ protease and phosphatase inhibitor (ThermoFisher # 78430) and centrifuged to separate debris from the lysate. The lysate was first pre-cleared with unconjugated agarose resin to remove any proteins that may bind non-specifically to the resin. It was then incubated with the conjugated resins for 2 hours at 4°C, after which the spin-tubes containing the mixture were placed in a spin column and washed 5 times. Proteins bound to AvFc were eluted from the column using a low pH buffer. Several elutions were performed, and each fraction was pooled together and neutralized with 1 M tris. To identify the proteins that had bound to AvFc, the solution was submitted for proteomic analysis by Liquid Chromatography-Mass Spectrometry at the University of Louisville Proteomics Core. The Scaffold Viewer proteomic software with Gene Ontology (GO) was used to analyze the LC-MS data. Proteins identified in the $AvFc^{lec-}$ sample were discarded from the analysis. Additionally, GO keywords were used to trim the dataset to include only membrane-bound glycoproteins.

MTS Assay

B16F10 cells were grown as described above. 5,000 cells were plated into each well of a 96-well plate. Cells were then exposed to AvFc or AvFc^{lec-} beginning at 3 µM with 1:5 serial dilutions. Multiple wells were left for use as a no-drug control. Plates were incubated for 48 hours at 37°C, at which point 20 µL of MTS reagent was added to each well (Abcam ab197010). Plates were read each hour for 5 hours at 495 nm. Absorbance values were converted to percent viability, using the no-drug control as 100% viability. These values were then plotted against concentration and fit with a non-linear regression using GraphPad Prism.

Scratch Cell Migration Assay

Migration of B16F10 cells in response to AvFc was measured using a scratch cell migration assay, also called a wound-healing assay. B16F10 cells were grown on a 6-well plate until confluency, at which point they were serum starved for 6-8 hours. After starvation, each well was scratched twice using a pipette tip and washed with PBS to remove floating cells. Each well was then filled with serum-free media containing AvFc at 0.12, 0.6, or 3 µM or AvFc^{lec-} at 3 µM. One well was used as a no-drug control. Two lines perpendicular to the scratches were made in each well to give a reference point when imaging the scratches. An inverted fluorescent microscope was used to image the scratches at 0, 17, 41, and 64 hours. The area of the scratch was then calculated using ImageJ, and percentage of area closed was calculated and plotted against time.

Pharmacokinetics of AvFc in C57bl/6 Mice

The pharmacokinetics of AvFc in mice was evaluated using 4 groups of 4 mice each, per gender. At time 0, all animals were given a 25 mg/kg dose of AvFc intraperitoneally. Blood was sampled at two time points per group of 4 mice (0.5 and 8 hours, 1 and 24 hours, 2 and 48 hours, and 4 and 72 hours), using the submandibular vein for the first small draw and euthanasia/cardiac puncture for the second. Serum was then assayed for AvFc using a gp120 ELISA, which had been validated in the presence of mouse serum (no major matrix effects were detected). Serum concentration was plotted against time, and PK parameters were estimated using PK Solver [74].

A549-GFP Lung Cancer Model

The A549-GFP lung cancer model was carried out using 20 NOD.CB17-Prkdc^{scid}/J (or NOD-SCID) or 20 B6.CB17-Prkdc^{scid}/SzJ (or SCID) mice. A549-GFP cells were grown in DMEM with 10% FBS. On day 0, animals were split evenly into groups of 10 and given either vehicle or AvFc at 25 mg/kg intraperitoneally. After 2-4 hours, 2 x 10^6 A549-GFP cells were injected intravenously. Dosing continued every other day for a total of six doses. After 28 days animals were euthanized, and their lungs imaged with a fluorescence-capable camera. Fluorescence was quantified using ImageJ, and any gray value under 100 was considered to be background.

Experimental Animals

All animal work was conducted with approval by the University of Louisville Institutional Animal Care and Use Committee and in concordance with its policies. All animals were housed in dedicated facilities with free access to food and water and acclimatized to the environment for 1 week prior to beginning any study. Animals were routinely monitored for health, and euthanasia

performed when human endpoints were met or at the conclusion of the study. Asphyxiation with CO_2 was used as the primary method of euthanasia, followed by cervical dislocation as an adjunct method.

CHAPTER III: RESULTS

Anti-SIV Activity of AvFc

The anti-SIV activity of AvFc was first explored using an *in vitro* neutralization assay. Three highly pathogenic strains of SIV were donated from Dr. Francois Villinger's group at the New Iberia Research Center at the University of Louisiana, Lafayette: smE660, isolated from the African sooty mangabey, and mac239 and mac251, which were isolated from macaques. These strains were chosen as they are commonly used in HIV/SIV vaccine studies and in macaque challenge models as they are capable of establishing a disease similar to AIDS in monkeys. AvFc was capable of neutralizing all three strains of the virus (**Figure 7**) with IC_{50} values of 15.3 nM (smE660), 6.6 nM (mac239), and 1.8 nM (mac251). These values are comparable to though slightly higher than the average IC_{50} obtained against primary HIV strains using PBMCs as the target cell (0.3 nM; Hamorsky, Kouokam, Dent et al. submitted). Conversely, $AvFc^{lec-}$ was incapable of neutralizing the virus, indicating that neutralization occurred due to the binding of HMG structures on SIV gp120. A representative curve for this is shown in **Figure 7.**

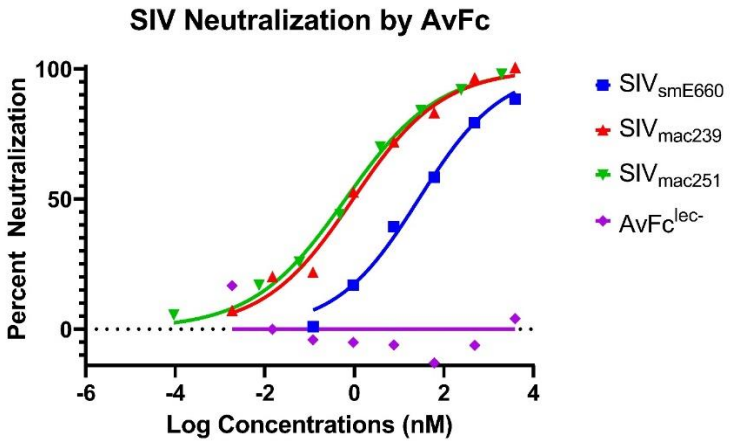

Figure 7 - SIV Neutralization by AvFc. Neutralization of primary SIV was measured as a decrease in luminescent signal in a TZM-bl assay. AvFc was capable of neutralizing SIV smE660, mac239, and mac251 with IC_{50} values in the low nanomolar range (15.3, 6.6, and 3.8 nM respectively). Conversely, $AvFc^{lec-}$ was incapable of neutralizing the virus. A representative curve for the 3 strains and for the negative control are shown above.

Next, flow cytometry was used to determine whether or not AvFc could recognize SIV-infected cells. Cells isolated from macaque MLNs were infected with SIV_{mac251} and stained with AvFc and a goat anti-human IgG-FITC. As shown in **Figure 8**, AvFc bound and recognized infected cells at concentrations of 1 and 10 µg/mL. However, it was not able to bind to uninfected cells at 10 µg/mL, indicating that AvFc is specific for HMGs displayed on the surface of the infected cells. Being able to bind infected cells is necessary for the induction of ADCC and may improve the efficacy of AvFc in *in vivo* SIV-challenge models. To prepare for such a model, it was necessary to understand the pharmacokinetics of AvFc in a macaque so that an appropriate dosing regimen could be decided. Two female macaques were given a 21 mg intravenous bolus dose of AvFc (3.6 and 3.7 mg/kg), and serum was sampled at 0, 0.5, 1, 2, 4, 8, 24, 48, and 72 hours. Before serum could be assayed for AvFc by gp120 ELISA, we first had to determine whether or not macaque serum would interfere with its binding to gp120. A gp120 ELISA using varying concentrations of macaque serum from a commercial vendor spiked with AvFc showed no change in EC_{50}, LLOD, or LLOQ (**Figure 9**), indicating that there was no matrix effect on detection.

AvFc was detected in all macaque serum samples, except for time 0, and the resulting concentration vs. time curve indicated that AvFc has a half-life in macaques of 27.6 ± 3.5 hours, and a clearance rate of 7.8 ± 3.2 mL/hour. Other PK parameters can be seen in **Figure 10**. For a 25 mg/kg dose (considered to be a "high" dose for our purposes) in an average macaque (5.34 kg, 325 mL blood volume), AvFc would need to be dosed every 6 days to maintain a blood concentration of 130 nM, or roughly 10 µg/mL, which is the target concentration for SIV neutralization *in vivo.*

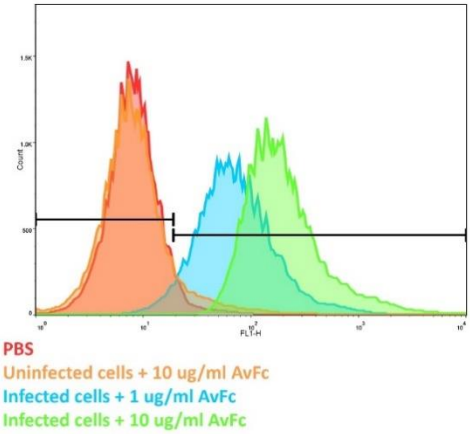

Figure 8 - Recognition of SIV-infected Macaque MLN cells by AvFc. SIV-infected macaque MLN cells were stained with AvFc and analyzed by flow cytometry. AvFc was able to detect infected cells at concentrations of 1 and 10 µg/mL, while conversely no positive signal was seen with uninfected cells stained with 10 µg/mL AvFc.

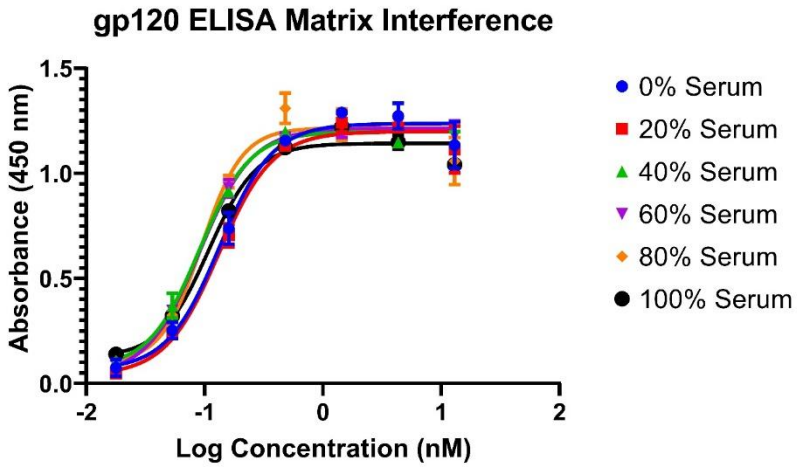

SERUM (%)	EC_{50} (nM)	LLOD (nM)	LLOQ (nM)
0	0.125	0.011	0.029
20	0.127	0.013	0.031
40	0.083	0.009	0.021
60	0.088	0.009	0.022
80	0.085	0.013	0.027
100	0.091	0.008	0.021

Figure 9 - Matrix Interference by Macaque Serum in the gp120 ELISA. A standard gp120 ELISA was performed by spiking AvFc into varying concentrations of macaque serum. No significant change in EC_{50}, LLOD, or LLOQ was seen, indicating that the inclusion of serum would not diminish the ability to detect AvFc.

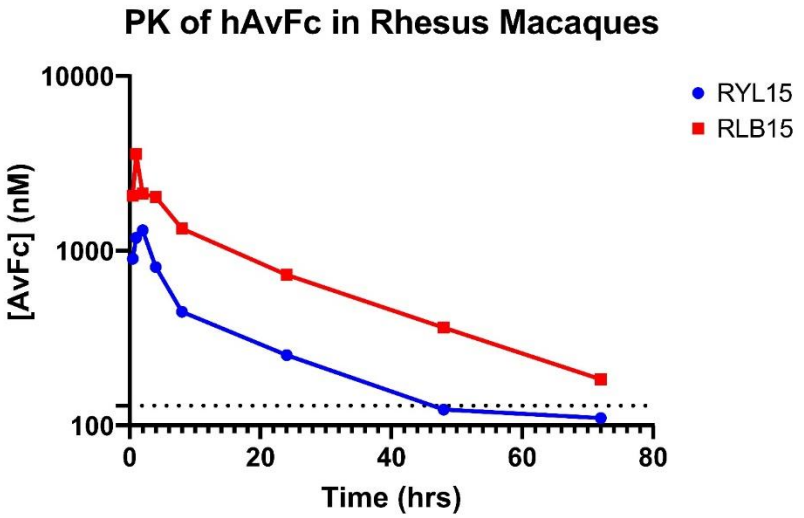

RYL15			RBL15		
Parameter	**Unit**	**Value**	**Parameter**	**Unit**	**Value**
Lambda z	1/h	0.0223	Lambda z	1/h	0.0287
$t_{1/2}$	h	31.1	$t_{1/2}$	h	24.2
t_{max}	h	2	t_{max}	h	1
C_{max}	µg/ml	100.93	C_{max}	µg/ml	275.94
C_0	µg/ml	69.36	C_0	µg/ml	159.38
C_{last}/C_{max}		0.0843	C_{last}/C_{max}		0.0513
AUC_{0-t}	µg/ml*h	1523.7	AUC_{0-t}	µg/ml*h	4036.3
$AUC_{0-\infty}$	µg/ml*h	1905.3	$AUC_{0-\infty}$	µg/ml*h	4529.8
$AUC_{0-t/0-\infty}$		0.7997	$AUC_{0-t/0-\infty}$		0.8911
$AUMC_{0-\infty}$	µg/ml*h^2	76152.3	$AUMC_{0-\infty}$	µg/ml*h^2	135017.2
MRT $_{0-\infty}$	h	39.97	MRT $_{0-\infty}$	h	29.81
V_z	(mg)/(µg/ml)	0.4942	V_z	(mg)/(µg/ml)	0.1616
CL	(mg)/(µg/ml)/h	0.01102	CL	(mg)/(µg/ml)/h	0.00464
V_{ss}	(mg)/(µg/ml)	0.44052	V_{ss}	(mg)/(µg/ml)	0.13818

Figure 10 - Pharmacokinetic Analysis of AvFc in Rhesus Macaques. Top, the concentration vs. time curve of AvFc in macaque serum after a single intravenous bolus dose of 21 mg of AvFc. The dotted line indicates 130 nM, or 10 µg/mL, the goal concentration for SIV neutralization *in vivo* (at least 10x the IC_{50}). The bottom tables show the PK parameter output from the PK Solver software, which gives an average half-life of about 27.7 hours.

Anti-HCV Activity of AvFc

The anti-HCVcc activity of AvFc was evaluated in an immunofluorescence assay using replication-permissive Huh7.5 cells and replication competent J6/JFH-1 virus (genotype 2a). AvFc was capable of neutralizing the virus with an IC_{50} value of 2.4 nM, a potency similar to what

has been seen with HIV and SIV (see above). A representative neutralization curve is shown in **Figure 11**.

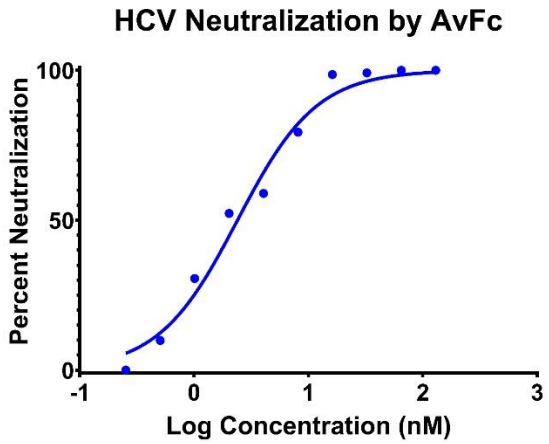

Figure 11 - HCV Neutralization by AvFc. Neutralization of HCV by AvFc was measured as a reduction in infectious foci in an immunofluorescence assay using Huh7.5 cells as the target cell. AvFc was able to neutralize the virus with an IC_{50} of 2.4 nM, similar to values obtained against SIV and HIV.

Anti-Cancer Activity of AvFc

It has previously been demonstrated that AvFc is capable of binding to a number of cancer-cell lines and inducing ADCC, owing to the expression of HMGs on the surface of many types of cancer (Figure 6). To expand on this, we used the B16F10 mouse melanoma lung metastasis model to determine whether or not the protein has any *in vivo* efficacy. First, however, we had to determine whether or not it was capable of recognizing the cell line. The binding to B16F10 cells was evaluated using flow cytometry, which showed over 80% of cells being bound at 130 nM and 50% at 20.3 nM (**Figure 12**). Binding to B16F10 cells also allowed for the induction of ADCC, demonstrated using an FcγRIIIa-luc-expressing Jurkat reporter cell line, with an EC_{50} of 1.51 nM (**Figure 13**). At the highest concentrations tested, AvFc elicited approximately a 4-fold increase in luciferase expression. The ability of the drug to bind and elicit

ADCC justified the further use of AvFc in the B16F10 melanoma lung metastasis model, which would demonstrate any *in vivo* activity.

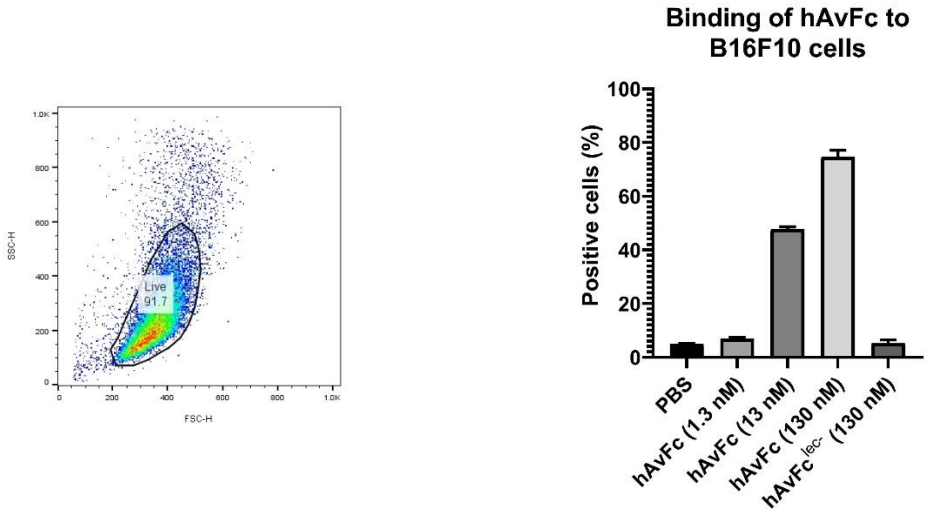

Figure 12 - Binding of AvFc to B16F10. The binding of AvFc to B16F10 mouse melanoma cells was evaluated using flow cytometry and a single-color FITC stain. Live cells were gated from the 100,000 total cells that were counted (left panel). The PBS-only control was then used to gate for FITC+ cells. At the highest concentration tested (130 nM), AvFc bound to approximately 80% of the cells. The EC_{50} of AvFc binding was determined to be 20.3 nM, calculated by non-linear regression using GraphPad Prism.

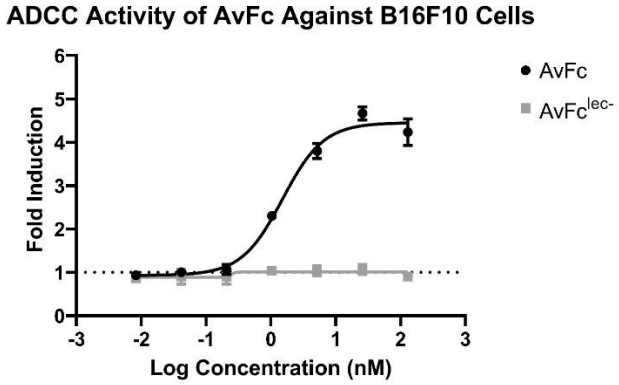

Figure 13 - ADCC Activity of AvFc Against B16F10 Cells. B16F10 cells, plated in a 96-well plate, were incubated with AvFc and a reporter cell line which expresses luciferase upon engagement of FcγRIIIa, which is the primary receptor responsible for inducing ADCC. As shown above, AvFc is capable of inducing ADCC in a dose-dependent manner with an EC_{50} value of 1.51 nM. The mutant $AvFc^{lec-}$, which cannot bind HMGs, was incapable of inducing ADCC.

In this model, 2.5 x 10^5 B16F10 cells were injected IV and AvFc, a non-sugar-binding mutant $AvFc^{lec-}$, or a vehicle was administered to mice concurrently and every other day

afterwards for a total of 6 doses. No significant changes in body weight or behavior were seen in any of the treatment groups, indicating that the drug was well tolerated with little acute toxicity (data not shown). On day 21, lungs isolated from the treated mice displayed significantly fewer nodules than the vehicle control (**Figure 14**). Furthermore, lungs isolated from the AvFc^{lec-} group did not show such a decrease, indicating that AvFc specifically was responsible for the anti-cancer activity seen. When treatment was delayed however, the results were less clear. Treatment of mice 7 days after IV injection of B16F10 cells did appear to improve mouse survival slightly, but non-significantly (**Figure 15**). Likewise, using a B16F10 flank tumor model, in which 2.5x10^5 cells were injected into the hind-left flank of the animal and treatment was delayed until the tumors became visible, a significant delay in tumor growth by day 14 was seen (**Figure 16**). The total effect on the tumor was modest however, and treatment did not prevent them from growing.

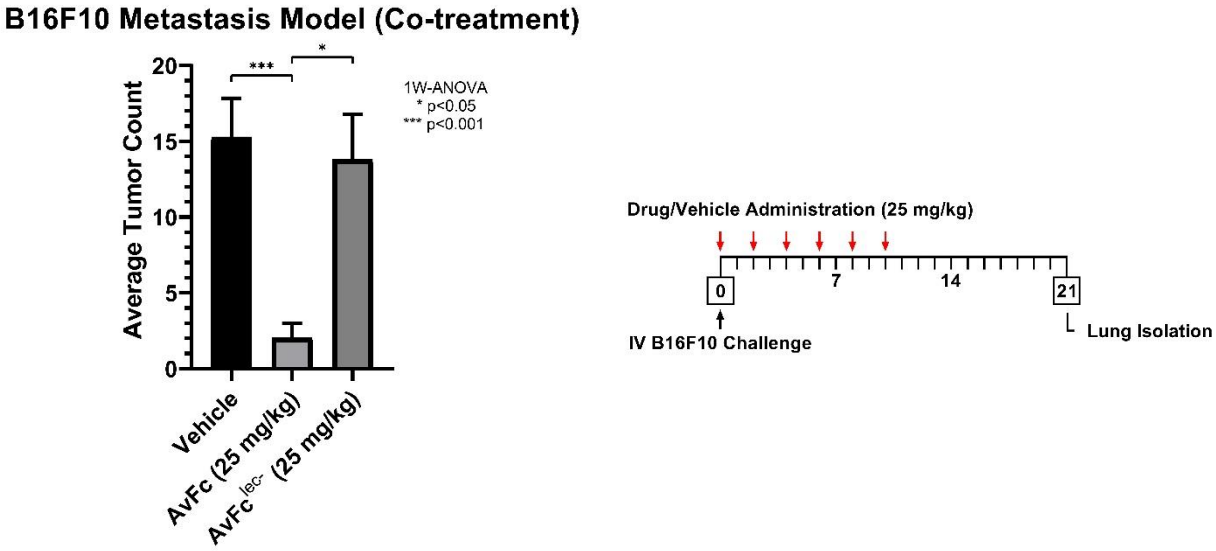

Figure 14 - B16F10 Melanoma Metastasis Model, Co-treatment with AvFc. On day 0, 250,000 B16F10 cells were injected IV into 8-10 week old C57bl/6 mice. The treatment was begun the same day as the cells were administered and continued every other day for a total of 6 doses. On day 21, lungs were isolated and the number of tumor nodules counted. While the mutant, non-HMG-binding AvFc^{lec-} was unable to prevent the formation of tumors in the lung, AvFc at the same dose significantly reduced the number of lung nodules. Data were analyzed by 1-way ANOVA, with multiple comparison's corrected with Tukey's range test.

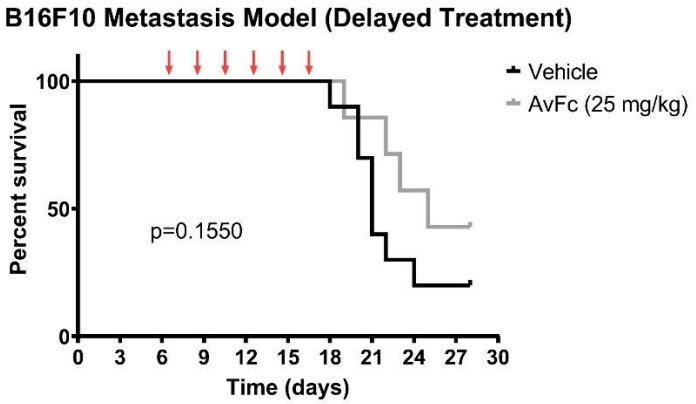

Figure 15 - B16F10 Melanoma Metastasis Model, Delayed Treatment with AvFc. Using the same melanoma metastasis model as in **Figure 14**, but by delaying treatment for 7 days, we found that AvFc did not significantly improve the survival of C57bl/6 mice (p=0.1550, Gehan-Breslow-Wilcoxon test). However, there was a trend towards increased survival which may be resolved with a larger sample size or more optimal dosing regimen. No differences in the lung nodules were noted.

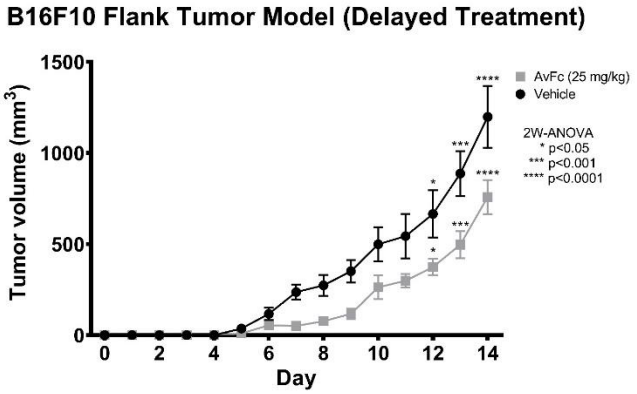

Figure 16 - B16F10 Flank Tumor Model with Delayed Treatment. In this model, mice were given 250,000 B16F10 cells in the hind left flank subcutaneously and dosed with AvFc beginning when the tumors became visible (day 5). Dosing continued every other day until day 14. A delay in tumor growth was noted and a significant decrease in average tumor volume was seen beginning on day 12. Data were analyzed by 2-way ANOVA with multiple comparisons corrected using Tukey's range test.

A number of experiments were then conducted to elucidate the possible anti-cancer mechanism of AvFc. One possibility is that AvFc targets a specific receptor or receptors, resulting in anti-cancer activity. Co-immunoprecipitation of A549, H460 (lung cancers), HL-60, and K562 (blood cancers) cell lysates with AvFc or the mutant $AvFc^{lec-}$ led to the identification of several surface markers that may be targeted by the drug (**Table 1**). EGFR, SORL1, IGF1R, LRP1,

CNTNAP1, and LRP10 were all identified in both of the lung cancer cell lines. EGFR is the target of several approved monoclonal antibody immunotherapies for lung cancer, including cetuximab. IGF1R on the other hand, is the target of several experimental antibody immunotherapies, though none have been approved to date [75-78]. Thus, it is possible that part of AvFc's mechanism may be due to the targeting of these receptors, and indeed data produced in our laboratory (not shown) seems to agree with this. Common between the two blood cancers was LAMP1 and ICAM1. Adhesion molecules like ICAM1 may play a role in cell metastasis and malignancy, and so it is hypothetically possible that AvFc may interact with these kinds of molecules to affect cancer-cell movement [79]. Lastly, a number of receptors were found to be common to all four of the cell-lines tested, including IGF2R, PLXNB2, NPC1, and M6PR. Particularly, IGF2R and M6PR are known to be mutated in some cancer types [80]. Based on these results, it seems possible that AvFc may be targeting some specific receptors on the cell surface to elicit its anti-cancer activity.

Found in both lung cancer cell-lines

Gene Name	Accession	Molecular Weight
Cluster of Epidermal growth factor receptor GN=EGFR	sp|P00533|EGFR_HUMAN	134 kDa
Cluster of Sortilin-related receptor GN=SORL1	sp|Q92673|SORL_HUMAN	248 kDa
Cluster of Insulin-like growth factor 1 receptor GN=IGF1R	sp|P08069|IGF1R_HUMAN	155 kDa
Prolow-density lipoprotein receptor-related protein 1 GN=LRP1	sp|Q07954|LRP1_HUMAN	505 kDa
Contactin-associated protein 1 GN=CNTNAP1	sp|P78357|CNTP1_HUMAN	156 kDa
Low-density lipoprotein receptor-related protein 10 GN=LRP10	sp|Q7Z4F1|LRP10_HUMAN	76 kDa

Found in both blood cancer cell-lines

Gene Name	Accession	Molecular Weight
Lysosome-associated membrane glycoprotein 1 OS=Homo sapiens GN=LAMP1	sp|P11279|LAMP1_HUMAN	45 kDa
Intercellular adhesion molecule 1 GN=ICAM1	sp|P05362|ICAM1_HUMAN	58 kDa

Found in all four cancer cell-lines

Gene Name	Accession	Molecular Weight
Cation-independent mannose-6-phosphate receptor GN=IGF2R	sp|P11717|MPRI_HUMAN	274 kDa
Plexin-B2 GN=PLXNB2	sp|O15031|PLXB2_HUMAN	205 kDa
Niemann-Pick C1 protein GN=NPC1	sp|O15118|NPC1_HUMAN	142 kDa
Cation-dependent mannose-6-phosphate receptor GN=M6PR	sp|P20645|MPRD_HUMAN	31 kDa
Integrin alpha-5 GN=ITGA5	sp|P08648|ITA5_HUMAN	115 kDa

Table 1 - Identification of the Cell-surface Binding Partners of AvFc. Co-immunoprecipitation was performed with AvFc or a negative control, $AvFc^{lec-}$, on cancer-cell lysates from 4 cell lines: A549, H460, HL-60, and K562. Proteins were then identified using mass spectrometry. Those that were identified both in the negative control samples and in the AvFc samples were removed from the final analysis, as were any proteins identified that were not integral plasma membrane proteins (as determined by gene ontology keywords and literature search). The most immediately interesting binding partners identified were EGFR, IGFR1, and IGFR2, which are known to be upregulated or improperly functioning in many cancers. AvFc was also found to bind a number of adhesion molecules and transporters.

To explore the non-Fc-mediated anti-cancer activity of the drug, the viability of B16F10 cells and their ability to migrate in the presence of AvFc was then explored using MTS and scratch cell-migration assays. In the MTS assay, AvFc only showed cytotoxicity at the highest concentrations tested (0.6 and 3 µM), with an EC_{50} value of 9.7 µM (**Figure 17**). At similar concentrations however, no anti-migratory effect was seen in the cell-migration assay (**Figure 18**). This seems to indicate that, at least with the cell lines and concentrations tested, that AvFc has little innate anti-cancer activity arising simply from the Avaren portion binding to its target. Furthermore, based on a pharmacokinetic study of AvFc in C57bl/6 mice it would be unlikely that the protein reached such high concentrations in the blood of mice in the B16F10 challenge studies. A single 25 mg/kg dose of AvFc showed a peak blood concentration of about 2.5 µM in males and 1.9 µM in females, far lower than even the EC_{50} of the drug in the MTS assay. It may be possible to increase C_{max} by dosing every day, given that the half-life of the drug was determined to be 25.4 hours in males and 18.5 hours in females (**Figure 19**).

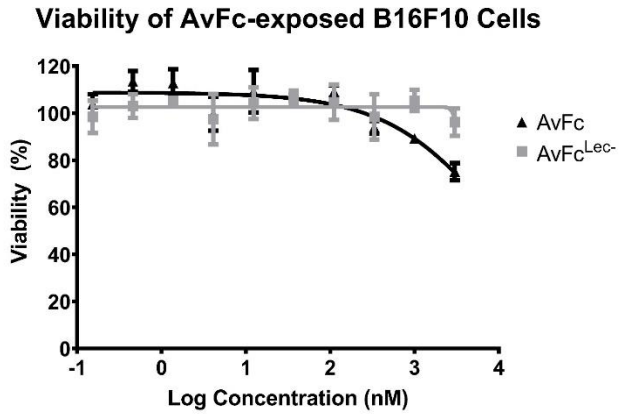

Figure 17 - Effect of AvFc Exposure on B16F10 Viability. Varying concentrations of AvFc were added to 5,000 B16F10 cells on a 96-well plate beginning at 3 µM. Cells were exposed to AvFc for 48 hours, at which point the MTS reagent was added to the wells and incubated for 3 hours at 37°C. While AvFc^{lec-} was unable to elicit any cytotoxicity at any concentration, AvFc showed moderate cytotoxicity at the highest concentrations with an estimated EC_{50} of 9.7 µM.

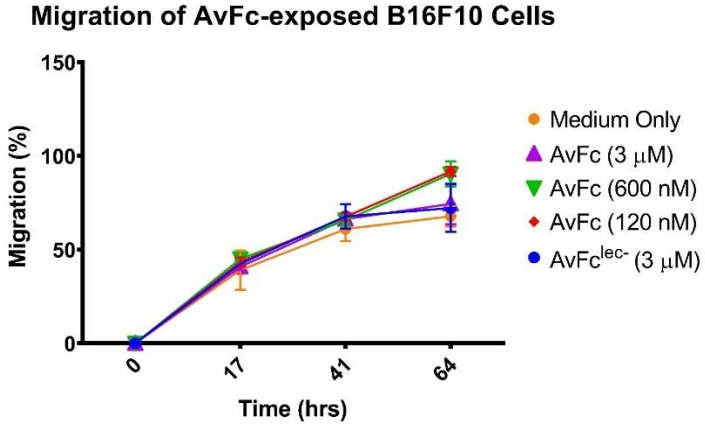

Figure 18 - Migration of AvFc-exposed B16F10 cells. The migration of B16F10 cells during exposure to varying concentrations of AvFc was evaluated by a scratch assay on a 6 well plate. No concentration of AvFc was able to prevent the cell migration into the scratched area.

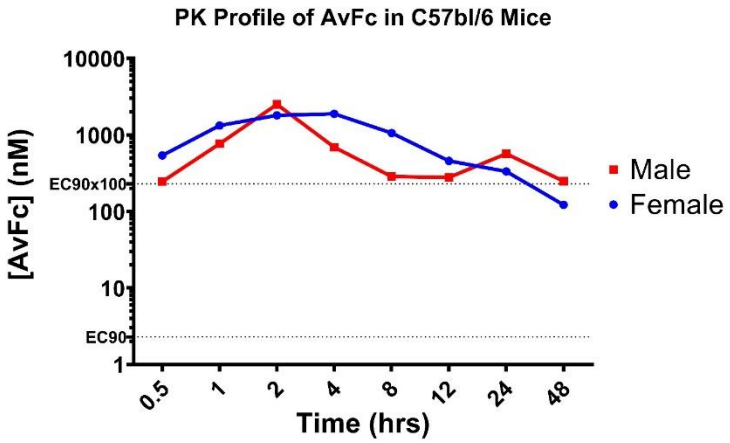

Male			Female		
Parameter	**Unit**	**Value**	**Parameter**	**Unit**	**Value**
Lambda z	1/h	0.0273	Lambda z	1/h	0.037
$t_{1/2}$	h	25.4	$t_{1/2}$	h	18.5
t_{max}	h	2	t_{max}	h	4
C_{max}	nmol/L	2507.667	C_{max}	nmol/L	1886.4
C_{last_obs}/C_{max}		0.0989	C_{last_obs}/C_{max}		0.0647
AUC_{0-t}	nmol/L*h	23083.6	AUC_{0-t}	nmol/L*h	24967.3
$AUC_{0-\infty}$	nmol/L*h	32164.7	$AUC_{0-\infty}$	nmol/L*h	28226.6
$AUC_{0-t/0-\infty}$		0.718	$AUC_{0-t/0-\infty}$		0.885
$AUMC_{0-\infty}$	nmol/L*h^2	1208450.5	$AUMC_{0-\infty}$	nmol/L*h^2	564592.6
$MRT_{0-\infty}$	h	37.57	$MRT_{0-\infty}$	h	20.00
Vz/F_{obs}	(µg)/(nmol/L)	0.569	Vz/F_{obs}	(µg)/(nmol/L)	0.473
Cl/F_{obs}	(µg)/(nmol/L)/h	0.0155	Cl/F_{obs}	(µg)/(nmol/L)/h	0.0177

Figure 19 - Pharmacokinetics of AvFc in C57bl/6 Mice. Top, the concentration vs. time curve of AvFc in C57bl/6 serum after a single intraperitoneal dose of 500 µg. The two dotted lines represent the EC_{90} of AvFc's ADCC activity against B16F10 cells and that value times 100, which we use as the target concentration that we wish to maintain in the blood. To achieve this concentration, a 500 µg dose of AvFc should be given every 48 hours or so. The bottom tables show the PK parameter output from the PK Solver software, with the average half-life estimated as approximately 22 hours. Based on the C_{max}, the average weight of a 10-week old C57bl/6 mouse (25.6 for males, 19.8 for females) and the average blood volume (79 mL/kg), the bioavailability was calculated as 78% for males and 45% for females.

To demonstrate the necessity of AvFc's Fc effector functions to its anti-cancer activity, an A549-GFP lung cancer model was employed using two strains of immunocompromised mice: NOD.CB17-Prkdc^{scid}/J (or NOD-SCID) and B6.CB17-Prkdc^{scid}/SzJ (or SCID) (**Figure 20**). These cells stably and constitutively express GFP, allowing for their detection *ex-vivo*. With co-treatment with AvFc, no significant decrease in lung GFP intensity was seen in the NOD-SCID mice, which

lack B, T, and functional NK cells. However, a significant decrease was seen in the SCID mice, which lack B and T cells but retain NK cells. Since NK cells are the primary effector cells for ADCC, it appears that their presence is necessary for AvFc to exert its anti-cancer activity at least in this particular model.

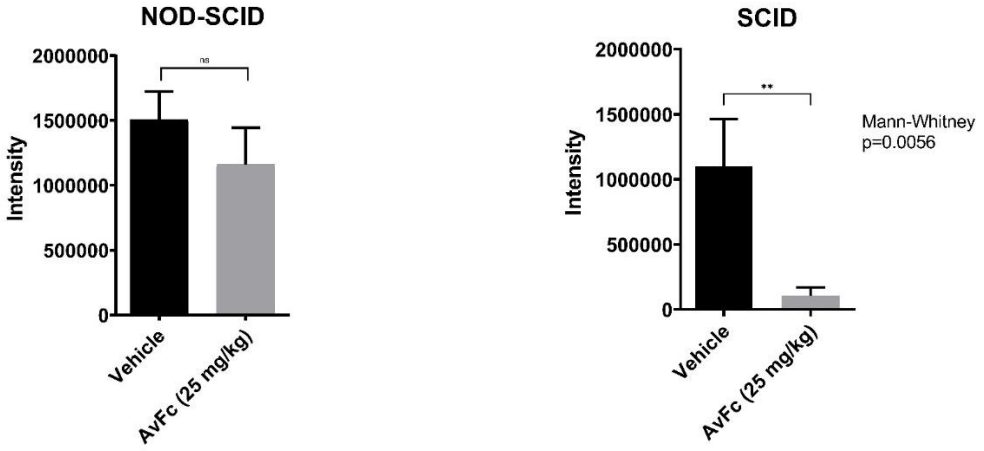

Figure 20 - A549-GFP Lung Cancer Model, Co-treatment with AvFc. In this model, mice were given $2x10^6$ A549-GFP cells and co-treated with AvFc at 25 mg/kg beginning on day 0 and continuing every other day for six doses. On day 28, animals were euthanized and the GFP intensity in the lungs quantified by fluorescent imaging and ImageJ. The same model was done in SCID and NOD-SCID mice. In NOD-SCID mice, AvFc did not show any efficacy, though it did in SCID mice, indicating that Fc functions are important for AvFc's mechanism.

CHAPTER IV: DISCUSSION

It is becoming clear that aberrant glycosylation brought on by certain viruses and cancer may be a useful biomarker or pharmaceutical target, and the goal of this work was to demonstrate that targeting HMGs with a specific carbohydrate-binding-agent (CBA) is a possible therapeutic approach. To date, there are only a handful of CBAs in clinical development and one approved drug – dinutuximab – which is an anti-GD2 disialoganglioside mAb for the treatment of certain high-risk pediatric neuroblastomas [81]. Even fewer agents are capable of binding specifically to disease-associated HMGs. For example, HMGs from gp120 make up a significant portion of the epitope of the HIV bNAb 2G12 [82], though the remainder of it is formed by the underlying protein limiting the bNAbs activity to HIV-1. Another antibody, TM10, was found to bind much more specifically to HMGs and was even capable of recognizing multiple cancer cell-lines [83]. However, there was little *in vivo* efficacy largely due to the fact that the antibody is an M class immunoglobulin, which primarily remains in the vasculature and has little to no effector function. A potential solution to the above limitations may be the development of a novel CBA that can target HMGs specifically and make use of Fc-mediated effector functions. This makes AvFc a first in class molecule which may be well suited for this purpose, owing to its high specificity for HMGs and HMG-bearing viruses and cancer cells and its inclusion of the Fc region of human IgG1 which allows for efficient induction of effector functions.

As demonstrated in this work, AvFc can neutralize SIV and HCV, owing to the fact that the envelope proteins of these viruses contain dense arrays of HMGs on their surface. SIVmac239, for example, contains 27 sites while the E1 and E2 proteins of HCV contain 15,

which cover their surfaces and serve as a glycan shield hiding the underlying protein structure from the immune system. AvFc appears to have little to no affinity for either the disaccharide α1,2-mannobiose or the glycan Man9 individually (data not shown). Instead, it appears that AvFc requires not only the presence of these glycans but requires a certain density of them so as to engage all three of the sugar binding sites at once, as has been demonstrated for the parent lectin actinohivin [cite Tanaka et al PNAS paper]. Additionally, AvFc may interact with multiple glycans on the surface of the virus with being specific to any particular one, the implication of this being that AvFc could neutralize any virus that displays a high number of HMGs. This however is not the case. Viruses such as Middle East respiratory syndrome coronavirus (MERS-CoV) or Ebola, both of which have HMG-rich glycoproteins that AvFc can indeed bind to (measured by Biacore, not shown), are nonetheless resistant to neutralization by it. Thus, it seems that it is not just the presence or absence of HMGs that determines whether or not AvFc can bind and neutralize a virus but rather it is the spatial arrangement of those glycans on the viral surface in the context of virus-host interaction; these glycans must be located on or near integral entry or fusion domains so as to block their action during infection. What remains to be explored is where exactly on HIV gp120 or HCV E1/E2 AvFc is binding to that allows it to neutralize those viruses, and not others with similar properties.

The primary barrier to an HIV cure is the presence of latent viral reservoirs, which harbor proviral DNA in the host cell chromosome that do not express antigen and are not eliminated by antiretroviral therapy. Much work has been done to identify agents that can reactivate the virus and allow for the recognition and elimination of infected cells (latency reversal agents, LRAs), with the major candidates belonging to the group of histone deacetylase inhibitors like romidepsin [84]. No single LRA has been identified that can decrease the size of the viral reservoir, thus it is likely that a combination therapy consisting of an LRA and a bNAb is

necessary for effective treatment [64]. In order for this to be effective, the bNAb must be able to recognize infected cells and effectively elicit ADCC. To date, few descriptions of antibodies that are capable of this have been published [65, 85-87]. As demonstrated in this work, AvFc can effectively recognize SIV-infected MLN cells isolated from rhesus macaques (**Figure 8**), opening up the possibility that any SIV-infected cells can be targeted and possibly eliminated through ADCC *in vivo* in combination with an LRA. Further studies are needed to assess the effects of AvFc on the latent reservoir.

The present study demonstrated that AvFc has anti-cancer activity in multiple models though the exact mechanism is not known. Unlike contemporary cancer immunotherapies like cetuximab, AvFc does not have a single protein target on the surface of the cell and, based on co-immunoprecipitation data, may interact with a number of surface receptors, adhesion molecules, and transporters that display HMGs (**Table 1**). Despite effective binding to cancer cells, AvFc does not seem to be cytotoxic or disrupt cell migration except at very high concentrations (> 1 μM, **Figure 17**, **Figure 18**). This would seem to imply that Fc-mediated effector functions, and not direct cell inhibition, are necessary for its anti-cancer activity. This hypothesis is supported by the fact that little activity is seen in the A549 cancer model only in SCID mice and not in NOD-SCID mice, which are deficient in NK cells and other innate cells (**Figure 20**). Further studies are warranted to confirm the hypothesis and to refine the Fc-mediated antitumor activity of AvFc, particularly through the use of variants of AvFc with modified Fc regions. Changes to the amino acid sequence or to the glycan profile of the Fc region can increase or decrease its affinity to the various FcγRs. One well-characterized Fc mutant is GASDALIE (G236A/S239D/A330L/I332E), which increases the affinity of antibodies to FcγRI and FcγRIIIa. This mutation has been shown to increase the protection conferred by monoclonal antibodies in mouse models of cancer and infectious disease [88-90]. Removal of

the core fucose in the glycan located at the single *N*-glycosylation site in the CH2 domain of the Fc region also increases the affinity for FcγRIIIa and allows for a stronger elicitation of ADCC [91]. Conversely, mutation of the abrogates binding to FcγRs and limits ADCC activity [92]. Further studies with AvFc should incorporate these mutants to demonstrate whether or not AvFc's primary anti-cancer mechanism is through ADCC.

REFERENCES

1. Khoury, G.A., R.C. Baliban, and C.A. Floudas, *Proteome-wide post-translational modification statistics: frequency analysis and curation of the swiss-prot database.* Scientific Reports, 2011. **1**: p. 90.
2. Pamela Stanley, N.T., Markus Aebi, *N-Glycans*, in *Essentials of Glycobiology [Internet]. 3rd edition.* 2017, Cold Spring Harbor Laboratory Press: NY.
3. Cherepanova, N., S. Shrimal, and R. Gilmore, *N-linked glycosylation and homeostasis of the endoplasmic reticulum.* Current opinion in cell biology, 2016. **41**: p. 57-65.
4. van Ree, R., *Carbohydrate Epitopes and Their Relevance for the Diagnosis and Treatment of Allergic Diseases.* International Archives of Allergy and Immunology, 2002. **129**(3): p. 189-197.
5. Vigerust, D.J. and V.L. Shepherd, *Virus glycosylation: role in virulence and immune interactions.* Trends Microbiol, 2007. **15**(5): p. 211-8.
6. Kreisman, L.S. and B.A. Cobb, *Infection, inflammation and host carbohydrates: a Glyco-Evasion Hypothesis.* Glycobiology, 2012. **22**(8): p. 1019-1030.
7. Kornfeld, R. and S. Kornfeld, *Assembly of asparagine-linked oligosaccharides.* Annu Rev Biochem, 1985. **54**: p. 631-64.
8. Pinho, S.S. and C.A. Reis, *Glycosylation in cancer: mechanisms and clinical implications.* Nature Reviews Cancer, 2015. **15**: p. 540.
9. Christiansen, M.N., et al., *Cell surface protein glycosylation in cancer.* Proteomics, 2014. **14**(4-5): p. 525-546.
10. Sharon, N. and H. Lis, *History of lectins: from hemagglutinins to biological recognition molecules.* Glycobiology, 2004. **14**(11): p. 53R-62R.
11. Balzarini, J., et al., *Profile of resistance of human immunodeficiency virus to mannose-specific plant lectins.* J Virol, 2004. **78**(19): p. 10617-27.
12. Wyatt, R., et al., *The antigenic structure of the HIV gp120 envelope glycoprotein.* 1998. **393**(6686): p. 705.
13. Alvarez, C.P., et al., *C-type lectins DC-SIGN and L-SIGN mediate cellular entry by Ebola virus in cis and in trans.* Journal of virology, 2002. **76**(13): p. 6841-6844.
14. Ritchie, G., et al., *Identification of N-linked carbohydrates from severe acute respiratory syndrome (SARS) spike glycoprotein.* 2010. **399**(2): p. 257-269.
15. Walls, A.C., et al., *Glycan shield and epitope masking of a coronavirus spike protein observed by cryo-electron microscopy.* 2016. **23**(10): p. 899.
16. Vieyres, G., et al., *Characterization of the envelope glycoproteins associated with infectious hepatitis C virus.* 2010. **84**(19): p. 10159-10168.

17. Inokoshi, J., et al., *Molecular cloning of actinohivin, a novel anti-HIV protein from an actinomycete, and its expression in Escherichia coli.* Biochemical and biophysical research communications, 2001. **281**(5): p. 1261-1265.
18. Boyd, M.R., et al., *Discovery of cyanovirin-N, a novel human immunodeficiency virus-inactivating protein that binds viral surface envelope glycoprotein gp120: potential applications to microbicide development.* Antimicrobial agents and chemotherapy, 1997. **41**(7): p. 1521-1530.
19. Koshte, V., et al., *Isolation and characterization of BanLec-I, a mannoside-binding lectin from Musa paradisiac (banana).* 1990. **272**(3): p. 721-726.
20. Mori, T., et al., *Isolation and characterization of griffithsin, a novel HIV-inactivating protein, from the red alga Griffithsia sp.* Journal of Biological Chemistry, 2005. **280**(10): p. 9345-9353.
21. Bokesch, H.R., et al., *A potent novel anti-HIV protein from the cultured cyanobacterium Scytonema varium.* 2003. **42**(9): p. 2578-2584.
22. Huskens, D., et al., *Microvirin, a novel α (1, 2)-mannose-specific lectin isolated from Microcystis aeruginosa, has comparable anti-HIV-1 activity as cyanovirin-N, but a much higher safety profile.* 2010: p. jbc. M110. 128546.
23. O'Keefe, B.R., et al., *Scaleable manufacture of HIV-1 entry inhibitor griffithsin and validation of its safety and efficacy as a topical microbicide component.* Proc Natl Acad Sci U S A, 2009. **106**(15): p. 6099-104.
24. Nixon, B., et al., *Griffithsin protects mice from genital herpes by preventing cell-to-cell spread.* J Virol, 2013. **87**(11): p. 6257-69.
25. O'Keefe, B.R., et al., *Broad-spectrum in vitro activity and in vivo efficacy of the antiviral protein griffithsin against emerging viruses of the family Coronaviridae.* J Virol, 2010. **84**(5): p. 2511-21.
26. Meuleman, P., et al., *Griffithsin has antiviral activity against hepatitis C virus.* Antimicrobial agents and chemotherapy, 2011: p. AAC. 00633-11.
27. Ishag, H.Z., et al., *Griffithsin inhibits Japanese encephalitis virus infection in vitro and in vivo.* Arch Virol, 2013. **158**(2): p. 349-58.
28. Tsai, C.-C., et al., *Cyanovirin-N inhibits AIDS virus infections in vaginal transmission models.* AIDS research and human retroviruses, 2004. **20**(1): p. 11-18.
29. Tsai, C.-C., et al., *Cyanovirin-N gel as a topical microbicide prevents rectal transmission of SHIV89. 6P in macaques.* AIDS research and human retroviruses, 2003. **19**(7): p. 535-541.
30. Lagenaur, L.A., et al., *Prevention of vaginal SHIV transmission in macaques by a live recombinant Lactobacillus.* 2011. **4**(6): p. 648.
31. Barrientos, L.G., et al., *Cyanovirin-N binds to the viral surface glycoprotein, GP1,2 and inhibits infectivity of Ebola virus.* Antiviral Res, 2003. **58**(1): p. 47-56.
32. Munkley, J. and D.J. Elliott, *Hallmarks of glycosylation in cancer.* Oncotarget, 2016. **7**(23): p. 35478.
33. Liu, B., et al., *Induction of apoptosis by Polygonatum odoratum lectin and its molecular mechanisms in murine fibrosarcoma L929 cells.* 2009. **1790**(8): p. 840-844.

34. Li, C., et al., *Molecular switch role of Akt in Polygonatum odoratum lectin-induced apoptosis and autophagy in human non-small cell lung cancer A549 cells.* 2014. **9**(7): p. e101526.
35. Ouyang, L., et al., *Polygonatum odoratum lectin induces apoptosis and autophagy via targeting EGFR-mediated Ras-Raf-MEK-ERK pathway in human MCF-7 breast cancer cells.* 2014. **21**(12): p. 1658-1665.
36. Podlech, O., et al., *Fermented mistletoe extract as a multimodal antitumoral agent in gliomas.* 2012. **2012**.
37. Lyu, S.Y., S.H. Choi, and W.B.J.A.o.p.r. Park, *Korean mistletoe lectin-induced apoptosis in hepatocarcinoma cells is associated with inhibition of telomerasevia mitochondrial controlled pathway independent of p53.* 2002. **25**(1): p. 93.
38. Hong, C.-E., et al., *Synergistic anticancer effects of lectin and doxorubicin in breast cancer cells.* 2014. **394**(1-2): p. 225-235.
39. Liu, B., M.-w. Min, and J.-K.J.A. Bao, *Induction of apoptosis by Concanavalin A and its molecular mechanisms in cancer cells.* 2009. **5**(3): p. 432-433.
40. Lei, H.-Y. and C.-P.J.J.o.b.s. Chang, *Lectin of Concanavalin A as an anti-hepatoma therapeutic agent.* 2009. **16**(1): p. 10.
41. Kunze, E., et al., *Long-term administration of galactoside-specific mistletoe lectin in an animal model: no protection against N-butyl-N-(4-hydroxybutyl)-nitrosamine-induced urinary bladder carcinogenesis in rats and no induction of a relevant local cellular immune response.* 2000. **126**(3): p. 125-138.
42. Schumacher, U., S. Feldhaus, and U.J.C.l. Mengs, *Recombinant mistletoe lectin (rML) is successful in treating human ovarian cancer cells transplanted into severe combined immunodeficient (SCID) mice.* 2000. **150**(2): p. 171-175.
43. Hamorsky, K.T., et al., *Rapid and scalable plant-based production of a cholera toxin B subunit variant to aid in mass vaccination against cholera outbreaks.* PLoS neglected tropical diseases, 2013. **7**(3): p. e2046.
44. Landry, N., et al., *Preclinical and clinical development of plant-made virus-like particle vaccine against avian H5N1 influenza.* PloS one, 2010. **5**(12): p. e15559.
45. Nandi, S., et al., *Techno-economic analysis of a transient plant-based platform for monoclonal antibody production.* mAbs, 2016. **8**(8): p. 1456-1466.
46. Aviezer, D., et al., *A plant-derived recombinant human glucocerebrosidase enzyme--a preclinical and phase I investigation.* PloS one, 2009. **4**(3): p. e4792-e4792.
47. Mason, H.S., D.M. Lam, and C.J. Arntzen, *Expression of hepatitis B surface antigen in transgenic plants.* Proceedings of the National Academy of Sciences of the United States of America, 1992. **89**(24): p. 11745-11749.
48. Hiatt, A., R. Cafferkey, and K. Bowdish, *Production of antibodies in transgenic plants.* Nature, 1989. **342**(6245): p. 76-8.
49. Mason, H.S., et al., *Expression of Norwalk virus capsid protein in transgenic tobacco and potato and its oral immunogenicity in mice.* Proceedings of the National Academy of Sciences, 1996. **93**(11): p. 5335-5340.

50. Mason, H.S., et al., *Edible vaccine protects mice against Escherichia coli heat-labile enterotoxin (LT): potatoes expressing a synthetic LT-B gene.* Vaccine, 1998. **16**(13): p. 1336-1343.
51. Peyret, H. and G.P.J.P.b.j. Lomonossoff, *When plant virology met Agrobacterium: the rise of the deconstructed clones.* 2015. **13**(8): p. 1121-1135.
52. Moore, L., K. Hamorsky, and N. Matoba, *Production of recombinant cholera toxin b subunit in Nicotiana benthamiana using GENEWARE® tobacco mosaic virus vector*, in *Recombinant Proteins from Plants*. 2016, Springer. p. 129-137.
53. Chilton, M.-D., et al., *Agrobacterium rhizogenes inserts T-DNA into the genomes of the host plant root cells.* 1982. **295**(5848): p. 432.
54. Gleba, Y., V. Klimyuk, and S. Marillonnet, *Magnifection—a new platform for expressing recombinant vaccines in plants.* Vaccine, 2005. **23**(17): p. 2042-2048.
55. Pogue, G.P., et al., *Production of pharmaceutical‐grade recombinant aprotinin and a monoclonal antibody product using plant‐based transient expression systems.* 2010. **8**(5): p. 638-654.
56. Lai, H., et al., *Robust production of virus‐like particles and monoclonal antibodies with geminiviral replicon vectors in lettuce.* 2012. **10**(1): p. 95-104.
57. Castilho, A., et al., *Rapid high yield production of different glycoforms of Ebola virus monoclonal antibody.* 2011. **6**(10): p. e26040.
58. Hamorsky, K.T., et al., *Efficient single tobamoviral vector-based bioproduction of broadly neutralizing anti-HIV-1 monoclonal antibody VRC01 in Nicotiana benthamiana plants and utility of VRC01 in combination microbicides.* Antimicrobial agents and chemotherapy, 2013. **57**(5): p. 2076-2086.
59. Lai, H., et al., *Monoclonal antibody produced in plants efficiently treats West Nile virus infection in mice.* 2010. **107**(6): p. 2419-2424.
60. Klimyuk, V., et al., *Production of recombinant antigens and antibodies in Nicotiana benthamiana using 'magnifection'technology: GMP-compliant facilities for small- and large-scale manufacturing*, in *Plant Viral Vectors*. 2012, Springer. p. 127-154.
61. Chun, T.-W., et al., *Presence of an inducible HIV-1 latent reservoir during highly active antiretroviral therapy.* 1997. **94**(24): p. 13193-13197.
62. Siliciano, J.D., et al., *Long-term follow-up studies confirm the stability of the latent reservoir for HIV-1 in resting CD4+ T cells.* 2003. **9**(6): p. 727.
63. Hütter, G., et al., *Long-term control of HIV by CCR5 Delta32/Delta32 stem-cell transplantation.* New England Journal of Medicine, 2009. **360**(7): p. 692-698.
64. Rasmussen, T.A. and S.R. Lewin, *Shocking HIV out of hiding: where are we with clinical trials of latency reversing agents?* Curr Opin HIV AIDS, 2016. **11**(4): p. 394-401.
65. Halper-Stromberg, A., et al., *Broadly Neutralizing Antibodies and Viral Inducers Decrease Rebound from HIV-1 Latent Reservoirs in Humanized Mice.* Cell, 2014. **158**(5): p. 989-999.
66. *NIH Consensus Statement on Management of Hepatitis C: 2002.* NIH Consens State Sci Statements, 2002. **19**(3): p. 1-46.

67. Asselah, T., et al., *Direct‐acting antivirals for the treatment of hepatitis C virus infection: optimizing current IFN‐free treatment and future perspectives.* 2016. **36**: p. 47-57.
68. Manns, M.P. and T. von Hahn, *Novel therapies for hepatitis C — one pill fits all?* Nature Reviews Drug Discovery, 2013. **12**: p. 595.
69. Burgess, S., et al., *Drug interactions with direct-acting antivirals for hepatitis C: implications for HIV and transplant patients.* 2015. **49**(6): p. 674-687.
70. Chiba, H., et al., *Actinohivin, a novel anti-HIV protein from an actinomycete that inhibits syncytium formation: isolation, characterization, and biological activities.* Biochemical and biophysical research communications, 2001. **282**(2): p. 595-601.
71. Chiba, H., et al., *Actinohivin, a novel anti-human immunodeficiency virus protein from an actinomycete, inhibits viral entry to cells by binding high-mannose type sugar chains of gp120.* Biochemical and biophysical research communications, 2004. **316**(1): p. 203-210.
72. Todd, C.A., et al., *Development and implementation of an international proficiency testing program for a neutralizing antibody assay for HIV-1 in TZM-bl cells.* Journal of Immunological Methods, 2012. **375**(1): p. 57-67.
73. Reed, L.J. and H.J.A.j.o.e. Muench, *A simple method of estimating fifty per cent endpoints.* 1938. **27**(3): p. 493-497.
74. Zhang, Y., et al., *PKSolver: An add-in program for pharmacokinetic and pharmacodynamic data analysis in Microsoft Excel.* Computer Methods and Programs in Biomedicine, 2010. **99**(3): p. 306-314.
75. Anderson, P.M., et al., *A phase II study of clinical activity of SCH 717454 (robatumumab) in patients with relapsed osteosarcoma and Ewing sarcoma.* 2016. **63**(10): p. 1761-1770.
76. Curley, M.D., et al., *Istiratumab (MM-141), a bispecific antibody targeting IGF-1R and ErbB3, inhibits pro-survival signaling in vitro and potentiates the activity of standard of care chemotherapy in vivo in ovarian cancer models*. 2016, AACR.
77. Qu, X., et al., *Update of IGF-1 receptor inhibitor (ganitumab, dalotuzumab, cixutumumab, teprotumumab and figitumumab) effects on cancer therapy.* 2017. **8**(17): p. 29501.
78. Weyer-Czernilofsky, U., et al., *Xentuzumab, a humanized IGF-1 and IGF-2 ligand neutralizing antibody, improves the antitumor efficacy of enzalutamide in preclinical models of prostate cancer*. 2017, AACR.
79. Roland, C.L., et al., *ICAM-1 expression determines malignant potential of cancer.* 2007. **141**(6): p. 705-707.
80. Kong, F.-M., et al., *M6P/IGF2R is mutated in squamous cell carcinoma of the lung.* 2000. **19**(12): p. 1572.
81. Ploessl, C., et al., *Dinutuximab: an anti-GD2 monoclonal antibody for high-risk neuroblastoma.* 2016. **50**(5): p. 416-422.
82. Trkola, A., et al., *Human monoclonal antibody 2G12 defines a distinctive neutralization epitope on the gp120 glycoprotein of human immunodeficiency virus type 1.* 1996. **70**(2): p. 1100-1108.

83. Newsom-Davis, T.E., et al., *Enhanced Immune Recognition of Cryptic Glycan Markers in Human Tumors.* Cancer Research, 2009. **69**(5): p. 2018-2025.
84. Sogaard, O.S., et al., *The Depsipeptide Romidepsin Reverses HIV-1 Latency In Vivo.* PLoS Pathog, 2015. **11**(9): p. e1005142.
85. Cohen, Y.Z., et al., *Analysis of HIV-1 latent reservoir and rebound viruses in a clinical trial of anti-HIV-1 antibody 3BNC117.* 2018: p. 324509.
86. Bruel, T., et al., *Elimination of HIV-1-infected cells by broadly neutralizing antibodies.* Nature Communications, 2016. **7**: p. 10844.
87. Bar, K.J., et al., *Effect of HIV antibody VRC01 on viral rebound after treatment interruption.* 2016. **375**(21): p. 2037-2050.
88. Bournazos, S., et al., *Broadly Neutralizing Anti-HIV-1 Antibodies Require Fc Effector Functions for In Vivo Activity.* Cell, 2014. **158**(6): p. 1243-1253.
89. DiLillo, David J. and Jeffrey V. Ravetch, *Differential Fc-Receptor Engagement Drives an Anti-tumor Vaccinal Effect.* Cell, 2015. **161**(5): p. 1035-1045.
90. Smith, P., et al., *Mouse model recapitulating human Fcγ receptor structural and functional diversity.* Proceedings of the National Academy of Sciences, 2012. **109**(16): p. 6181-6186.
91. Liu, S.D., et al., *Afucosylated antibodies increase activation of FcγRIIIa-dependent signaling components to intensify processes promoting ADCC.* 2015. **3**(2): p. 173-183.
92. Arnold, J.N., et al., *The Impact of Glycosylation on the Biological Function and Structure of Human Immunoglobulins.* 2007. **25**(1): p. 21-50.

CURRICULUM VITAE

NAME:	Matthew William Dent
ADDRESS:	Department of Pharmacology and Toxicology 505 South Hancock Street Lab 626 Louisville, Kentucky 40202
DOB:	September 6, 1991
EDUCATION AND TRAINING:	B.S. Molecular Biosciences and Biotechnology Arizona State University 2010-2014
	M.Sc. Plant Genetics and Crop Improvement University of East Anglia 2014-2015
AWARDS:	Provost's Scholarship Award, 2010-2014
	B.S. awarded Magna Cum Laude, 2014
	ASU Sun Award, 2014
	1st place at Research!Louisville, Poster Competition, Category: Master's Basic Science Graduate Student

PUBLICATIONS:	Leuzinger, K., **Dent, M.*,** et al., Efficient agroinfiltration of plants for high-level transient expression of recombinant proteins. Journal of Visualized Experiments, 2013(77). * Co-first-author Chen, Q., et al., Agroinfiltration as an effective and scalable strategy of gene delivery for production of pharmaceutical proteins. Adv Tech Biol Med, 2013. 1(1). Chen, Q., et al. (2016). Transient protein expression by agroinfiltration in lettuce. Recombinant proteins from plants, Humana Press, New York, NY: 55-67. **Dent, M.**, et al., Plant-produced anti-dengue virus monoclonal antibodies exhibit reduced antibody-dependent enhancement of infection activity. Journal of General Virology, 2016. 97(12): p. 3280-3290. Yang, M., **Dent, M.*,** et al., Immunization of Zika virus envelope protein domain III induces specific and neutralizing immune responses against Zika virus. Vaccine, 2017. 35(33): p. 4287-4294. * Co-first-author Chen, Q., et al., Molecular Pharming: Plant-Made Vaccines. Molecular Pharming, 2018: p. 231-273. Kasinger, L., **Dent, M.*,** et al. (2019). A Novel Anti-HIV-1 Bispecific bNAb-Lectin Fusion Protein Engineered in a Plant-based Transient Expression System. Plant Biotech Journal. Accepted for publication * Co-first-author
NATIONAL/INTERNATIONAL POSTER PRESENTATIONS:	"Enhancing the tobacco chassis: applications of Cas9-based genome editing technologies to heterologous protein production in plants" – Poster given at Plant Based Vaccines, Antibodies, and Biologics in Lausanne, Switzerland (June 2015)